Helicons, Doppler-Shifted Cyclotron Resonance, and Gantmakher-Kaner Oscillations*

DAVID S. FALK

University of Maryland, College Park, Maryland 20742

AND

BILL GERSON

Howard University, Washington, D. C. 20001, and University of Maryland, College Park, Maryland 20742

AND

J. F. CAROLAN

University of British Columbia, Vancouver, British Columbia, Canada

(Received 27 August 1969)

The surface impedance of a metal slab, in the presence of a magnetic field normal to its surface, is studied. A model Fermi surface, which exhibits realistic properties, is considered and the various modes of the electromagnetic field (helicons, Doppler-shifted cyclotron resonance, Gantmakher-Kaner oscillations) are analytically examined separately in order to gain a greater understanding of the sources of these contributions. Variations of the basic model Fermi surface are then introduced. In particular, it is shown that, for a suitably designed partially compensated Fermi surface, it is possible to obtain high-frequency helicons at reasonable magnetic fields for metallic net carrier densities. A general hierarchy of cylindrically symmetric Fermi surfaces is presented, leading to a variety of Gantmakher-Kaner contributions.

I. INTRODUCTION

WHEN a metal is subjected to a dc magnetic field normal to its surface and an rf electromagnetic field tangential to its surface, the electric field inside the metal is quite complicated, depending on the method of excitation, the details of the surface scattering, and the shape of the Fermi surface, as well as the magnitudes of all the various parameters involved. Although formulas have been developed[1,2] for the electric field, and more specifically, for the surface impedance, realistic Fermi surfaces usually require that these formulas be evaluated numerically. It is thus rather difficult to see how the various aspects of the Fermi surfaces come into play in their effect on the different modes of the electromagnetic field.

The purpose of this work is to examine various models of Fermi surfaces which are sufficiently complicated that they exhibit realistic properties, and yet which are sufficiently simple that the analysis can be carried through analytically. This enables us to look separately at the various modes, helicons,[3–7] Doppler-shifted

cyclotron resonance (DSCR),[8,9] and Gantmakher-Kaner (GK) oscillations,[10] and to examine how each of them can be affected by appropriate Fermi surfaces. In particular, it suggests the types of Fermi surface that can produce anomalous effects in the surface impedance. It also allows us to clear up some confusion about the amplitude of the GK oscillations.

We begin, in Sec. II, with a discussion of how the electric field and surface impedance are calculated for several different methods of excitation, once one knows the conductivity. All of our discussions will be confined to the assumption that the electrons in the metal are specularly reflected at the surface of the metal. However, we will indicate where diffuse boundary conditions would be expected to give qualitatively different results.

In Sec. III, we will evaluate the conductivity for our basic model Fermi surface. This model, suggested by Copper in the [111] direction, contains necks and velocity maxima and will serve as the central core of the work. After separating the contributions of the different modes to the electric field in Sec. IV, and examining the pole contributions (helicon, DSCR) in Sec. V and the branch cut contribution (GK oscillations) in Sec. VI, we shall consider how these are modified by various modifications of the Fermi surface. Thus, in Sec. VII we shall consider compensation effects and show how, under appropriate circumstances, they may give rise to high-frequency helicons at the usual experimental magnetic fields, while in Sec. VIII we shall consider a variety of other, but related, Fermi surfaces. The distinction, in Sec. VIII, will be primarily the nature of the branch-cut contribution. All model Fermi

* Work supported in part by the U. S. Air Force Office of Scientific Research under Grant No. AFOSR-68-1459, and the National Research Council of Canada.

[1] G. E. H. Reuter and E. H. Sondheimer, Proc. Roy. Soc. (London) **A195**, 336 (1948).

[2] P. M. Platzman and S. J. Buchsbaum, Phys. Rev. **132**, 2 (1963).

[3] P. Aigrain, in *Proceedings of the International Conference on Semiconductor Physics, Prague, 1960* (Academic Press Inc., New York, 1961), p. 224.

[4] O. V. Konstantinov and V. I. Perel, Zh. Eksperim. i Teor. Fiz. **38**, 161 (1960) [English transl.: Soviet Phys.—JETP **11**, 117 (1960)].

[5] R. Bowers, C. R. Legendy, and F. E. Rose, Phys. Rev. Letters **7**, 339 (1961).

[6] J. C. McGroddy, J. L. Stanford, and E. A. Stern, Phys. Rev. **141**, 437 (1966).

[7] S. J. Buchsbaum, in *Plasma Effects in Solids*, edited by J. Bok (Dunod Cie., Paris, 1965).

[8] P. B. Miller and R. R. Haering, Phys. Rev. **128**, 126 (1962).

[9] E. A. Stern, Phys. Rev. Letters **10**, 91 (1963).

[10] V. F. Gantmakher and E. A. Kaner, Zh. Eksperim. i Teor. Fiz. **48**, 1572 (1965) [English transl.: Soviet Phys.—JETP **21**, 1053 (1965)].

surfaces we use will have cylindrical symmetry about the direction of the magnetic field, but within this restriction a complete hierarchy of surfaces and attendant branch-cut contributions will be presented.

II. ELECTRIC FIELD AND SURFACE IMPEDANCE

We consider here a slab of metal of infinite transverse dimensions lying between $z=0$ and $z=L$. The rf electric field $\mathbf{E}$, propagating in the positive z direction with time dependence $e^{-i\omega t}$, and the electric current in the metal $\mathbf{j}$, both of which vary only in the z direction, are related by Maxwell's equation

$$\frac{d^2\mathbf{E}(z)}{dz^2} + \frac{\omega^2}{c^2}\mathbf{E}(z) = -\frac{4\pi i\omega}{c^2}\mathbf{j}(z). \quad (1)$$

To obtain another relation between the current and the field, we introduce the complex tensor conductivity $\bar{\sigma}$. For the case of an infinite sample, $\bar{\sigma}$ is translationally invariant and Ohm's Law takes a particularly simple form in terms of momentum components. Platzman and Buchsbaum[2] have shown, for the case of specularly reflecting boundaries, how to convert this slab problem to a bulk problem with periodic current sheets (i.e., discontinuities in $\mathbf{E}' \equiv d\mathbf{E}/dz$) at $z=nL$, with $\mathbf{E}$ even about any of these planes. We will therefore simply sketch the derivation. With

$$\mathbf{j}(q) = \int_{-\infty}^{\infty} e^{-iqz}\mathbf{j}(z)dz = \bar{\sigma}(q)\mathbf{E}(q), \quad (2)$$

Maxwell's equation (1) becomes

$$\left[-q^2 + \frac{\omega^2}{c^2}\right]\mathbf{E}(q) - 2\sum_{m=-\infty}^{\infty} e^{-2imLq}$$

$$\times [\mathbf{E}'(0+) - e^{-iqL}\mathbf{E}'(L-)] = -(4\pi i\omega/c^2)\bar{\sigma}(q)\mathbf{E}(q). \quad (3)$$

Noting that

$$\sum_{m=-\infty}^{\infty} e^{-2imLq} = \frac{\pi}{L}\sum_{n=-\infty}^{\infty} \delta(q-k_n), \quad (4)$$

where

$$k_n = n\pi/L, \quad (5)$$

we may write

$$\mathbf{E}(z) = \int_{-\infty}^{\infty} \frac{dq}{2\pi} e^{iqz}\mathbf{E}(q)$$

$$= -\frac{1}{L}\sum_{n=-\infty}^{\infty} e^{ik_n z}\left[k_n^2 - \frac{\omega^2}{c^2}\bar{\epsilon}(k_n)\right]^{-1}$$

$$\times [\mathbf{E}'(0+) - (-1)^n\mathbf{E}'(L-)], \quad (6)$$

where we have introduced the complex-tensor dielectric constant (suppressing any indication of its dependence on frequency) as follows:

$$\bar{\epsilon}(q) = 1 + (4\pi i/\omega)\bar{\sigma}(q). \quad (7)$$
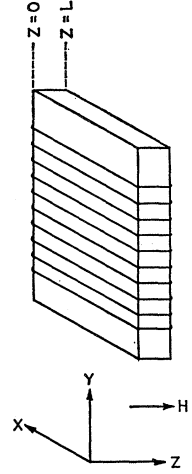

FIG. 1. Experimental arrangement for two-sided linearly polarized excitation showing rf coil and coordinate system used.

The tensor whose inverse we need in (6) will be diagonal, assuming the metallic lattice has at least three-fold symmetry about the z axis (i.e., the metal is cut with a symmetry direction normal to the surface) if we use the circularly polarized components of the electric field

$$E_\pm = E_x \pm iE_y, \quad (\pm\text{polarization}). \quad (8)$$

In order to go further with (6), we must state the experimental conditions, as they will relate $E'(0+)$ and $E'(L-)$. We shall consider two different situations.

A. One-Sided Circularly Polarized Excitation

This is the case considered by Platzman and Buchsbaum.[2] We take the incident wave coming from the left. The boundary condition is then that to the right of the slab there is only a free-space solution to the wave equation propagating to the right. That is

$$E_\pm'(L-)/E_\pm(L-) = i\omega/c. \quad (9)$$

If we let

$$f_\pm(z,L) \equiv -\frac{i\omega}{Lc}\sum_{n=0}^{\infty} \frac{(2-\delta_{n,0})\cos k_n z}{k_n^2 - (\omega^2/c^2)\epsilon_\pm(k_n)}, \quad (10)$$

where $\epsilon_\pm(k_n)$ are the appropriate diagonal elements of $\bar{\epsilon}(k_n)$, we get

$$E_\pm'(L-)/E_\pm'(0+) = f_\pm(L,L)/[1+f_\pm(0,L)] \quad (11)$$

and hence, the surface impedance for one-sided circularly polarized excitation

$$Z_\pm \equiv \frac{4\pi i\omega}{c^2}\frac{E_\pm(0+)}{E_\pm'(0+)} = \frac{4\pi}{c}\left(f_\pm(0,L) - \frac{f_\pm^2(L,L)}{1+f_\pm(0,L)}\right). \quad (12)$$

B. Two-Sided Antisymmetric Linearly Polarized Excitation

This is a commonly used experimental arrangement where the rf field is produced by a coil wrapped around
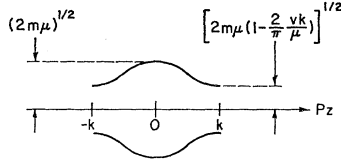
FIG. 2. Fermi surface (23). The surface is cylindrically symmetric about the p_z axis. Brillouin zone boundaries are at $p_z = \pm k$.

the sample[11] (Fig. 1). This necessarily implies that $\mathbf{E}(L-) = -\mathbf{E}(0+)$ and hence that

$$\mathbf{E}'(L-) = \mathbf{E}'(0+), \tag{13}$$

so that

$$\mathbf{E}(z) = -\frac{2}{L} \sum_{n=-\infty}^{\infty} e^{izk_{2n+1}}$$
$$\times \left(k_{2n+1}^2 - \frac{\omega^2}{c^2} \bar{\epsilon}(k_{2n+1}) \right)^{-1} \mathbf{E}'(0+), \tag{14}$$

which we may write in the form, for $z=0$,

$$\mathbf{E}(0+) = \sum_\nu T_{\mu\nu} E_\nu'(0+), \quad (\mu,\nu = x,y,z). \tag{15}$$

The condition of linear polarization implies that the rf magnetic field at the surface is linearly polarized, that is, $H_x(0+) = 0$. But,

$$(i\omega/c)H_x = E_y'. \tag{16}$$

Hence,

$$E_y'(0+) = 0, \tag{17}$$

so that $E_x(0+) = T_{xx}E_x'(0+)$, or the surface impedance

$$Z_{xx} \equiv \frac{4\pi i\omega}{c^2} \frac{E_x(0+)}{E_x'(0+)} = \frac{4\pi i\omega}{c^2} T_{xx}. \tag{18}$$

Finally,

$$T_{xx} = \tfrac{1}{2}(T_+ + T_-), \tag{19}$$

where

$$T_\pm = -\frac{2}{L} \lim_{z\to 0+} \sum_{n=-\infty}^{\infty} e^{izk_{2n+1}}$$
$$\times \left[k_{2n+1}^2 - \frac{\omega^2}{c^2} \epsilon_\pm(k_{2n+1}) \right]^{-1}. \tag{20}$$

Thus, the different modes of excitation require different, although similar sums [(10) and (20)] to be evaluated. In order to evaluate them, we shall need expressions for the dielectric constant, or equivalently, using (7), the conductivity. Actually, since, for metals, the frequencies that we will be interested in are much smaller than the plasma frequency, we can neglect the displacement current and write

$$(\omega^2/c^2)\epsilon_\pm(q) \simeq (4\pi i\omega/c^2)\sigma_\pm(q). \tag{21}$$

---

[11] V. F. Gantmakher, in *Progress in Low Temperature Physics*, edited by C. J. Gorter (North-Holland Publishing Co., Amsterdam, 1967), Vol. V.

Before proceeding further with the sums, we shall therefore turn to the evaluation of the conductivity.

III. CONDUCTIVITY FOR MODEL FERMI SURFACE

The conductivity $\sigma_\pm(q,\omega)$, in the presence of a static magnetic field $\mathbf{H}$ for the case of a Fermi surface with cylindrical symmetry about the direction of $\mathbf{H}$ (which we call the z direction), is given by[12]

$$\sigma_\pm(q,\omega) = \frac{ie^2}{(2\pi)^2} \frac{eH}{c} \int_{\mathrm{FS}} \frac{dp_z}{\omega_c} \frac{v_\perp^2}{\omega + i/\tau \pm \omega_c - qv_z}. \tag{22a}$$

Here, $v_\perp$ and v_z are, respectively, the components of the velocity

$$\mathbf{v} = \partial E/\partial \mathbf{p}, \tag{22b}$$

transverse to and parallel to the magnetic field, p_z is the component of momentum parallel to the magnetic field, the integral is over those values of p_z which lie on the Fermi surface, τ is the scattering lifetime, and ω_c is the cyclotron frequency

$$\omega_c = \frac{2\pi eH}{c} \bigg/ \left(\frac{\partial A}{\partial E} \right)_{p_z}, \tag{22c}$$

where $A(p_z,E)$ is the cross-section area of a surface of constant energy E on a plane of constant p_z.

The model Fermi surface we shall consider here is defined by the surfaces of constant energy, in the vicinity of the Fermi energy μ, being given by (Fig. 2), (taking $\hbar = 1$),

$$E = p_\perp^2/2m + (2/\pi)kv \sin^2(\pi p_z/2k). \tag{23}$$

Here $\mathbf{p}_\perp$ is the component of momentum transverse to the z direction, while k and v are parameters with the dimensions of momentum and velocity, respectively. There will be necks of the Fermi surface at $p_z = (2n+1)k$ provided that $(2/\pi)vk < \mu$. We take the Brillouin zone boundaries at $p_z = \pm k$. This surface was suggested by the Fermi surface of Copper[13] with its necks along the [111] direction. Copper, however, also has six other necks which introduce interruptions in the electron orbits as well as various hole orbits. We will consider in Secs. VII and VIII surfaces which have these properties.

From (23), we have

$$\mathbf{v}_\perp = \frac{\partial E}{\partial \mathbf{p}_\perp} = \frac{1}{m} \mathbf{p}_\perp \tag{24}$$

and

$$v_z = \frac{\partial E}{\partial p_z} = v \sin\frac{\pi p_z}{k}. \tag{25}$$

Thus, v_z has a maximum magnitude, equal to v, at the

---

[12] R. G. Chambers, Phil. Mag. 1, 459 (1956).
[13] A. B. Pippard, Phil. Trans. Roy. Soc. London A250, 325 (1957).

points $p_z = \pm\frac{1}{2}k$. The cross-section area is given by

$$A(p_z,E) = 2m\pi[E - vk/\pi + (vk/\pi)\cos(\pi p_z/k)], \quad (26)$$

which implies by (22c) that

$$\omega_c = eH/mc, \quad (27)$$

independent of p_z. This last property will be common to all the models we will consider.

Inserting these results in (22), we get

$$\sigma_\pm(q,\omega) = \frac{ie^2}{\pi^2} \frac{k}{\Omega_\pm}\left(\mu - \frac{vk}{\pi}\right)\left[1 - \left(\frac{qv}{\Omega_\pm}\right)^2\right]^{-1/2} \quad (28)$$

Here,

$$\Omega_\pm = \omega \pm \omega_c + i/\tau \quad (29)$$

and the square root is defined so that the phase of its argument lies between $-\pi$ and π. If we notice that the density of electrons contained in this Fermi sea is given by

$$n = \frac{2}{(2\pi)^3}\int_{-k}^{k} \pi p_\perp^2 dp_z = \frac{mk}{\pi^2}\left(\mu - \frac{vk}{\pi}\right) \quad (30)$$

and introduce the plasma frequency ω_p by

$$\omega_p^2 = 4\pi ne^2/m, \quad (31)$$

we can write

$$\sigma_\pm(q,\omega) = \frac{i}{4\pi} \frac{\omega_p^2}{\Omega_\pm}\left[1 - \left(\frac{qv}{\Omega_\pm}\right)^2\right]^{-1/2}. \quad (32)$$

This exact expression for the conductivity, though rather simpler than that for a spherical Fermi sea, nevertheless, implies the existence of all the usual modes of the electric field: helicons, DSCR, and GK oscillations.

IV. SEPARATION OF MODES

We are now ready to evaluate the surface impedance of a metal with the Fermi surface (23). We shall do this for the case of two-sided antisymmetric linearly polarized excitations, although similar techniques could be used for one-sided circularly polarized excitation. Thus, we will want to use (32) in (18), (19), and (20).

We transform the summation in (20) to an integration by using the identity

$$\frac{1}{L}\sum_{n=-\infty}^{\infty} F(k_{2n+1}) = -\frac{1}{4\pi}\int_c dq \frac{F(q)e^{-iqL/2}}{\cos\frac{1}{2}qL}, \quad (33)$$

where the contour c encloses, in a counterclockwise direction, all the zeros of $\cos\frac{1}{2}qL$ (the points $q=k_{2n+1}$) but no other singularities that the integrand might have. We note that $q^2 - (\omega^2/c^2)\epsilon_\pm(q)$ has no zeros for real values of q. If all zeros of this function have $|\mathrm{Im}q| > \delta$, where δ is a positive infinitesmal, and if we assume that the lattice has reflection symmetry in the xy plane, so that $q^2 - (\omega^2/c^2)\epsilon_\pm(q)$ is even in q, then we

can write

$$T_\pm = \frac{i}{\pi}\int_{-\infty+i\delta}^{\infty+i\delta} dq\left(q^2 - \frac{4\pi i\omega}{c^2}\sigma_\pm(q)\right)^{-1}\tan\frac{1}{2}qL, \quad (34)$$

where we have used (21) under the assumption that $\omega \ll \omega_p$.

The integral in (34) could be evaluated numerically, and this approach would be best in the case of a real Fermi surface. However, with the simple conductivity (32), much of the work can be done analytically, and this allows us to separate the contributions of the various physically distinct components of the electric field. This can be seen by considering the integral in (34).

In addition to the poles of the integrand of $T_\pm$ which come from $\tan\frac{1}{2}qL$ and lie on the real axis (and consequently, below the contour), there are two other kinds of singularities.

Poles, collective modes. There are poles, where the denominator in (34) vanishes, at

$$q^2 = (\omega^2/c^2)\epsilon_\pm(q) = (4\pi i\omega/c^2)\sigma_\pm(q). \quad (35)$$

These correspond to modes of the electromagnetic field (eigenfrequencies of the wave equation) which will be propagating (if q is essentially real) or damped (if q has an appreciable imaginary part). The long wavelength propagating mode is the helicon.[3-7] There is also a DSCR mode[6,8,9] at shorter wavelengths and a damped helicon for the "wrong" circular polarization.

Branch cuts, single-particle modes. There are also branch cuts in the integrand of (34) at the branch cuts of $\sigma_\pm(q)$. The branch points, for Fermi surface (23), occur at

$$(qv)^2 = \Omega_\pm^2 = (\omega \pm \omega_c + i/\tau)^2. \quad (36)$$

As may be seen from (22), the branch cuts occur wherever

$$\omega - qv_z = \mp\omega_c - i/\tau, \quad (37)$$

which corresponds to the condition for a Doppler-shifted cyclotron resonance of an electron drifting along the z direction with velocity v_z. Since v is the maximum magnitude of v_z, the ends of the branch cuts (37) are given by (36). These branch cuts produce the Gantmakher-Kaner oscillations,[10] oscillations in the electric field which are carried into the metal by electrons with the maximum v_z, and whose amplitude is diminished by some power of the distance into the metal, the value of the power being dependent upon the nature of the branch cut (see Sec. VIII).

These two different types of contributions may be examined separately by distorting the contour of integration in (34) into the upper-half complex q plane. Since the contribution from the semicircle at infinity vanishes due to the q^2 in the denominator, the only contributions will come from the poles and branch cuts which lie above the original contour. In Fig. 3, we sketch
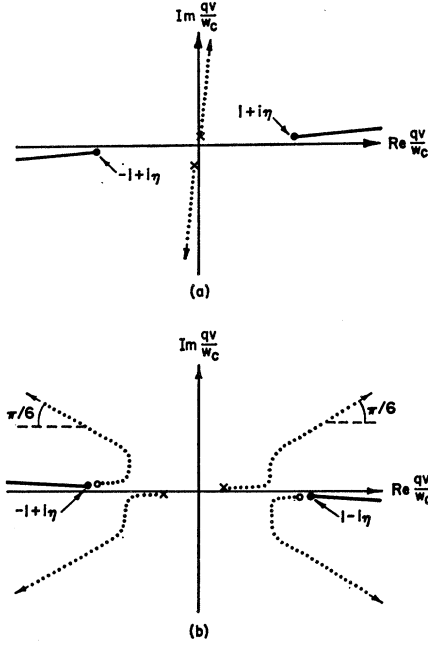
(a)

(b)

FIG. 3. Positions of singularities of integrand of (34) for Fermi surface (23). The solid lines are the branch cuts. The dotted lines indicate the paths followed by the poles as the magnetic field is decreased. Curves are sketched for $0 < \omega \ll \omega_c$ and $\omega_c \tau \gg 1$. Figure 3(a) is for the $+$ polarization and the pole corresponds to the damped helicon. Figure 3(b) is for the $-$ polarization. The crosses indicate the helicon pole positions, while the circles indicate the DSCR positions.

the positions of all the singularities for the case $0 < \omega \ll \omega_c$, $\omega_c \tau \gg 1$, in the complex q plane, where we measure q in units of ω_c/v. Figure 3(a) corresponds to the singularities in the integrand of T_+ while Fig. 3(b) corresponds to those in the integrand of T_-. Thus, T_+ contains the damped helicon (wrong polarization for $\omega > 0$), while T_- contains the helicon and the DSCR. We have indicated the paths along which the poles move as ω_c is decreased.

The contour of integration in (34) originally lay just above the real axis (above the poles of $\tan\frac{1}{2}qL$, which we have not indicated in the sketch) but below any of the singularities in the upper-half plane that are sketched in Fig. 3. The distorted contour of integration circles each of the singularities in the upper-half plane in a counterclockwise direction.

V. POLE TERMS

We first examine the contribution to (34) and hence to the surface impedance (18) that comes from those parts of the distorted contour that circle the poles in the upper-half plane (see Fig. 3). These poles occur at the roots of (35) which is the dispersion equation for the collective modes.

Inserting the conductivity (32), we have

$$q^2 = -(\omega_p^2\omega/\Omega_\pm c^2)[1-(qv/\Omega_\pm)^2]^{-1/2}. \qquad (38)$$

For the most part, we shall be dealing with frequencies $\omega \ll \omega_c$, so we may approximately write

$$\Omega_\pm \simeq \pm\omega_c(1\pm i/\omega_c\tau). \qquad (39)$$

It is convenient to introduce dimensionless parameters. To do this we measure lengths in units of v/ω_c which, to a factor of 2π, is the pitch of the helix described by the electrons with the maximum v_z along the magnetic field. We then define

$$z = qv/\omega_c, \quad \eta = 1/\omega_c\tau, \quad \text{and} \quad \xi^3 = \omega_p^2\omega v^2/\omega_c^3 c^2. \qquad (40)$$

(Throughout this paper we take $\omega > 0$, so $\xi^3 > 0$.) Then (38) becomes

$$\mp z^2/\xi^3 = [(1\pm i\eta)^2 - z^2]^{-1/2}, \quad (\pm\text{polarization}). \qquad (41)$$

The propagating modes correspond to those solutions of (41) for which z lies near the real axis. We can most easily see the nature of the roots in the collisionless limit ($\eta \to 0$) by plotting the two sides of (41) as functions of z^2. This is done in Fig. 4. Here, curve A is the right-hand side of (41), curve a is the left-hand side for $+$ polarization, while curves b, c, and d are the left-hand side for $-$ polarization for progressively larger values of ξ (larger values of ω or smaller values of H).

Since curves A and a do not intersect, we see that there is no real root for the "wrong" $+$ polarization. For the "correct" $-$ polarization, we see that there may be no roots (curve d) or two roots (curve b). There is a critical value of ξ, $\xi_m^6 = 4/27$, corresponding to curve c, which separates these regions. This corresponds to a magnetic field H_m. For $H > H_m$ we have $\xi < \xi_m$ and there are two roots; for $H < H_m$, we have $\xi > \xi_m$ and there are no roots. Just at H_m there is a double root. [By a root we mean a value of z^2 satisfying (41). This, of course, corresponds to two values of z, but only one is in the upper-half plane]. We thus identify H_m as the helicon edge, the minimum field for which helicon propagation is possible. (Note that at the edge, when $\xi = \xi_m$, the solution is $z^2 = \frac{2}{3}$. Thus $z^2 \neq 1$, $qv \neq \pm\omega_c$ at the helicon edge.)
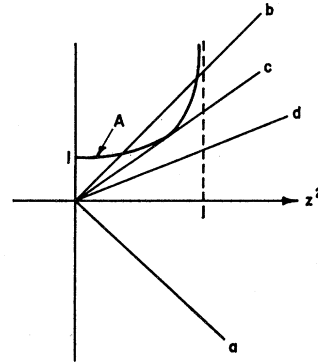

FIG. 4. Graphical solution of (41). Curve A is the right-hand side of (41). Curve a is the left-hand side for $+$ polarization. Curves b, c, and d are the left-hand side for $-$ polarization for progressively larger values of ξ (smaller H). Curve c corresponds to the edge.
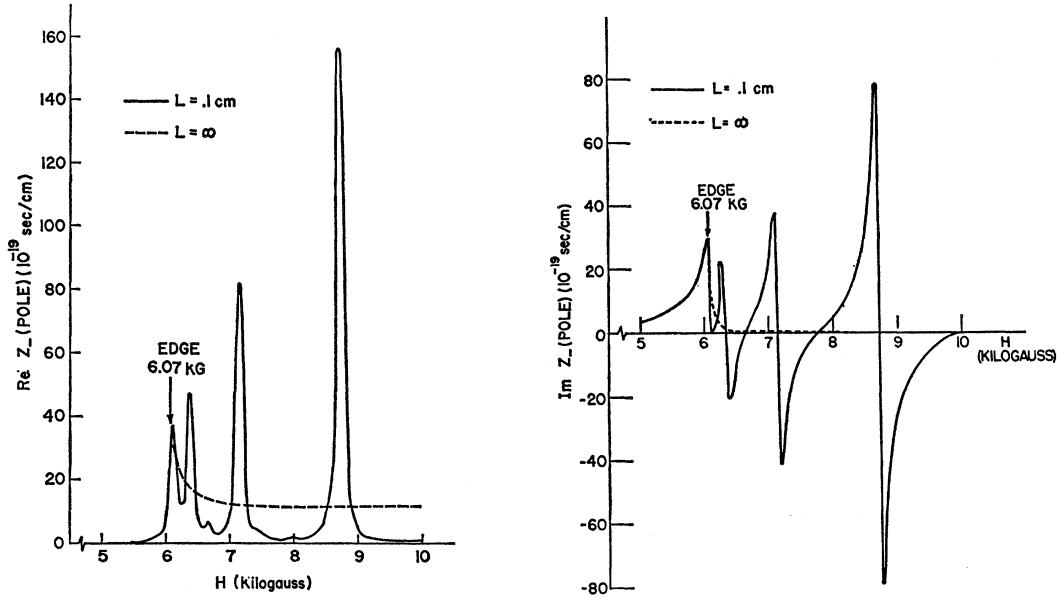
FIG. 5. Plots of the real (a) and imaginary (b) parts of the pole contribution to the surface impedance for $-$ polarization for the parameters (50). The helicon edge is at $H_m = 6.07$ kG. Dotted line is for the case of an infinitely thick sample ($L \to \infty$).

In this collisionless limit the solutions of (41) for both polarizations are obtained by solving

$$z^6 - z^4 + \xi^6 = 0. \tag{42}$$

The roots of (42) are

$$z_1{}^2 = \tfrac{1}{3}(1 - 2\cos\theta),$$

$+$polarization, damped helicon   (43a)

$$z_2{}^2 = \tfrac{1}{3}(1 + \cos\theta - \sqrt{3}\,\sin\theta),$$

$-$polarization, helicon   (43b)

$$z_3{}^2 = \tfrac{1}{3}(1 + \cos\theta + \sqrt{3}\,\sin\theta),$$

$-$polarization, DSCR,   (43c)

where

$$\cos 3\theta = (27/2)\xi^6 - 1. \tag{44}$$

For $H > H_m(\xi < \xi_m)$, θ is a real angle between $\tfrac{1}{3}\pi$ and 0, while for $H < H_m(\xi > \xi_m)$, θ becomes pure imaginary and all the roots are significantly displaced from the real axis.

The presence of a finite lifetime, $\eta \neq 0$, produces small imaginary parts in z_2 and z_3 even for $H > H_m$. The positions of these poles are indicated in Fig. 3, as well as the paths they move on as H is decreased.

The contributions of these poles to the surface impedance may be written as

$$Z_{xx}{}^{\text{pole}} = -\frac{4\pi i\omega v}{c^2 \omega_c} \sum_{j=1}^{3} \rho_j, \tag{45}$$

where ρ_j are the residues of the integral in (34) after the variable z has been introduced

$$\rho_j = \frac{\xi^6 \tan\tfrac{1}{2}\lambda z_j}{z_j(2\xi^6 - z_j{}^6)}. \tag{46}$$

Here,

$$\lambda = \omega_c L/v \tag{47}$$

is the thickness of the sample in units of the pitch.

It is sometimes of interest to separate the contributions of the $\pm$ polarizations to Z_{xx} according to

$$Z_{xx} = \tfrac{1}{2}(Z_+ + Z_-), \tag{48}$$

where

$$Z_\pm = (4\pi i\omega/c^2)T_\pm. \tag{49}$$

Then the pole corresponding to $j = 1$ contributes only to Z_+ while $j = 2$ and $j = 3$ contribute only to Z_-. To illustrate the pole contributions, we have plotted in in Fig. 5 the real and imaginary parts of $Z_-{}^{\text{pole}}$ for the following case.

An rf signal with $\omega = 2\pi \times 10^4$ sec^{-1} is incident on a sample of thickness $L = 0.1$ cm with parameters

$$v = 1.1 \times 10^8 \text{ cm/sec},$$
$$\omega_p{}^2 = 2.7 \times 10^{32} \text{ sec}^{-2},$$
$$\omega_c = 1.38H \times 10^{10} \text{ sec}^{-1},$$
$$\omega_c\tau = 20H, \tag{50}$$

where H is the magnetic field in kG.

The dispersion relation for the propagating modes ($-$ polarization for $\omega > 0$) may be written in the collisionless limit ($\eta \to 0$) as

$$\omega = (\omega_c c^2/\omega_p{}^2)q^2[1 - (qv/\omega_c)^2]^{1/2}. \tag{51}$$

This curve is sketched in Fig. 6. For small q one sees the classical helicon dispersion relation

$$\omega \simeq (\omega_c c^2/\omega_p{}^2)q^2. \tag{52}$$

The curve of ω versus q^2 departs from linearity in the
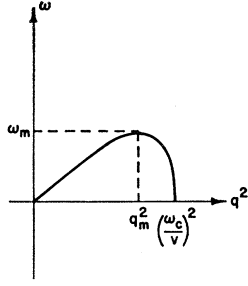
FIG. 6. Dispersion relation for the propagating modes (helicon and DSCR) in collisionless limit.

nonlocal region, and there is a maximum frequency ω_m for which propagation is possible. This frequency

$$\omega_m = (4/27)^{1/2}\omega_c{}^3c^2/\omega_p{}^2v^2 \qquad (53)$$

occurs for $q = q_m$, where

$$q_m{}^2 = \tfrac{2}{3}(\omega_c/v)^2. \qquad (54)$$

The dispersion curve bends over beyond q_m, terminating at the position of the DSCR

$$q^2 = (\omega_c/v)^2. \qquad (55)$$

The fact that ω vanishes as a square root at this point is peculiar to Fermi surfaces where the maximum $|v_z|$ (actually $|\partial A/\partial p_z|$) occurs for a finite cross-section area A.[6] In the case of the sphere, the maximum $|\partial A/\partial p_z|$ occurs at the pole of the sphere, where the cross-section area vanishes. The lack of electrons with the maximum $|\partial A/\partial p_z|$ in the sphere makes the DSCR too weak to bend over the helicon mode all the way to $\omega = 0$ at $q^2 = (\omega_c/v)^2$, although there is still a maximum ω_m at a smaller value of q^2 than (55). We shall return to this point in Sec. VIII. For the present Fermi surface (23), we see that both the helicon and the DSCR occur at all $\omega < \omega_m$ [that is, (51) is double valued for all $\omega < \omega_m$], becoming hybridized in the vicinity of q_m.

With regard to this last point, we should also plot ω versus q as we do in Fig. 7. The poles in the upper-half plane of Fig. 3(b) correspond to wave vectors of opposite sign for the helicon and DSCR. A glance at Fig. 7 shows that both modes have positive group velocity, propagating into the medium. The bending over of the helicon mode near q_m corresponds to hybridization with the DSCR which has negative group velocity (propagating up from the medium) but which, like the helicon, has positive phase velocity. This mode corresponds to the pole in the fourth quadrant of Fig. 3. Precisely at $q = q_m$, both modes have vanishing group velocity, and thus, as discussed in Ref. 6, produce a peak in the surface resistance, the edge anomaly (see Fig. 5).

Before discussing the behavior near the edge, we wish to examine the relative contributions of the helicon and the DSCR to the surface impedance at their respective resonances. To do this, we consider the dispersion relation (41) for small ξ^3 in the long mean free path limit ($\eta \ll 1$). The helicon and DSCR poles occur,

respectively, at

$$z_2 \simeq \xi^{3/2} + \tfrac{1}{2}i\xi^{3/2}\eta, \qquad (\xi, \eta \ll 1) \qquad (56a)$$

$$z_3 \simeq -1 + \tfrac{1}{2}\xi^6 + i\eta, \qquad (\xi, \eta \ll 1). \qquad (56b)$$

Hence, right at the geometrical resonances the tangent in (46) becomes approximately

$$\tan\tfrac{1}{2}\lambda z_2 \simeq 4i/\xi^{3/2}\lambda\eta, \qquad (\xi^{3/2}\lambda\eta \ll 1) \qquad (57a)$$

$$\tan\tfrac{1}{2}\lambda z_3 \simeq 2i/\lambda\eta, \qquad (\lambda\eta \ll 1). \qquad (57b)$$

[Note that the resonances occur when $\mathrm{Re}(\lambda z_j) = (2n+1)\pi$, and hence occur at different fields for the helicon, $j = 2$, and the DSCR, $j = 3$. When $\mathrm{Im}(\lambda z_j)$ becomes too large, of course, there no longer are resonances. This is the case with the damped helicon, $j = 1$]. Hence,

$$\rho_2 \simeq 2\xi^{-3/2}\tan\tfrac{1}{2}\lambda z_2 \simeq 2i/\xi^6\lambda\eta,$$

$$\text{(at helicon resonance)} \qquad (58a)$$

$$\rho_3 \simeq -\xi^6\tan\tfrac{1}{2}\lambda z_3 \simeq -2i\xi^6/\lambda\eta,$$

$$\text{(at DSCR resonance)}. \qquad (58b)$$

Thus we see, in this limit where $\xi \ll 1$, $\eta \ll 1$ and $\lambda\eta \ll 1$, that

$$\rho_3 \simeq -\xi^{12}\rho_2. \qquad (59)$$

Since $\xi^6 \leq \xi_m{}^6 = 4/27$ for any propagating modes, we must have

$$\xi^{12} < (4/27)^2 = 0.022 \qquad (60)$$

and therefore the peaks in the surface impedance due to the DSCR will be no larger than about 1% of the size of the peaks due to the helicon.

Returning to the behavior near the edge, we want to consider $\xi \simeq \xi_m$. Through the use of (41), (43), (45), (46), and (49), we can examine the surface impedance Z in the vicinity of the edge anomaly. Here it is convenient to let

$$\xi^6 = (2/27)(2+\epsilon), \qquad |\epsilon| \ll 1. \qquad (61)$$

For finite lifetimes, (41) may be rewriten as

$$z'^6 - z'^4 + \xi'^6 = 0, \qquad (62)$$

where

$$z' = z/(1-i\eta), \quad \xi' = \xi/(1-i\eta). \qquad (63)$$

Expanding the primed equivalent of (43), solving for z_2 and z_3, and inserting the results in (46), we eventually get the following expressions for the surface impedance in the limit of an infinitely thick sample so that the tangent in (46) can be replaced by i:

$$Z_- = 4\pi\frac{\omega v}{c^2\omega_c}\frac{1}{|\epsilon|^{1/2}}\left(1 - \frac{6i\eta}{\epsilon}\right), \qquad \eta \ll -\epsilon \quad (64a)$$

$$= (\pi\omega v/c^2\omega_c)(2/3\eta)^{1/2}(1+i), \qquad |\epsilon| \ll \eta \quad (64b)$$

$$= 4\pi i(\omega v/c^2\omega_c)\epsilon^{-1/2}(1-6i\eta/\epsilon), \qquad \eta \ll \epsilon. \quad (64c)$$

Throughout, we have taken $|\epsilon|$, $\eta \ll 1$. If the change in ξ is due to a change in ω, then

$$\epsilon \simeq 4(\omega - \omega_m)/\omega_m, \tag{65}$$

but if it is due to a change in H, then

$$\epsilon \simeq -12(H - H_m)/H_m. \tag{66}$$

The edge anomaly behavior as given by (64) and (66) can be seen in Fig. 5 for the case of the infinite sample as well as the finite sample. It is possible, for appropriate parameters, that q_m might be nearer a geometrical resonance of the finite sample, and thus distort that particular resonance, displacing it slightly. We should note, finally, that had we assumed diffuse scattering boundary conditions at the surface of the metal, the edge anomaly would be quite different.[14] In Appendix B, we exhibit the differences due to boundary conditions for a different Fermi-surface model.

VI. BRANCH-CUT CONTRIBUTIONS

We return now to a discussion of the remaining contributions to (34). When the contour in (34) is distorted into the upper-half plane, it encloses not only the poles that we have discussed in Sec. V, but also branch cuts (see Fig. 3). The portion of the surface impedance due to the integrals along the branch cuts arises from the Gantmakher-Kaner oscillations mentioned earlier. Taking account of the discontinuity across the cut, and writing that part of the surface impedance (49) due to the branch cuts as $Z_\pm^{GK}$, we may write the branch-cut contributions as

$$Z_\pm^{GK} = \mp \frac{8i\omega v}{c^2} \frac{\xi^3}{\omega_c(1 \pm i\eta)^4} I_\pm, \tag{67}$$

where

$$I_+ = I_-^* = \int_1^\infty dz \frac{(z^2-1)^{1/2}}{z^6 - z^4 + \xi'^6} \tan\tfrac{1}{2}\lambda'z, \tag{68}$$

with

$$\lambda' = \lambda(1 + i\eta), \quad \xi' = \xi/(1 + i\eta). \tag{69}$$

The occurrence of the tangent in (68) is due to the fact that we are treating a finite sample. The peaks of the tangent occur at the Fabry-Perot resonances. This can be seen directly by writing the tangent as

$$\tan\tfrac{1}{2}\lambda'z = -2 \sum_{n=-\infty}^{\infty} \frac{1}{\lambda z(1 + i\eta) - (2n+1)\pi}. \tag{70}$$

In the infinite collision time limit ($\eta \to 0$), the imaginary part of (70) becomes just a sum of δ functions at the Fabry-Perot resonances

$$\lambda z = qL = (2n+1)\pi. \tag{71}$$

For a sample which is not too thin, however, it is more convenient to expand the tangent in a series of

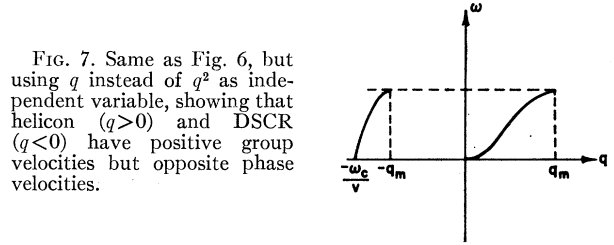[14] R. C. Alig, Phys. Rev. **165**, 833 (1968).

FIG. 7. Same as Fig. 6, but using q instead of q^2 as independent variable, showing that helicon ($q>0$) and DSCR ($q<0$) have positive group velocities but opposite phase velocities.

exponentials rather than use (70). Thus, we write

$$I_+ = \int_1^\infty dz \frac{(z^2-1)^{1/2}}{z^6 - z^4 + \xi'^6} - 2 \sum_{n=1}^\infty (-1)^n I_n, \tag{72}$$

where

$$I_n \equiv \int_1^\infty dz \frac{(z^2-1)^{1/2}}{z^6 - z^4 + \xi'^6} e^{in\lambda'z}. \tag{73}$$

This expansion corresponds to a multiple-reflection series[15] with the I_n falling off exponentially with nL/l, where l is the mean free path and

$$l = v\tau. \tag{74}$$

The first term in (72) does not oscillate with magnetic field. The integrals I_n can be evaluated in terms of known functions in the limit

$$\lambda = L\omega_c/v \gg 1. \tag{75}$$

This evaluation is performed in Appendix A with the result

$$I_n \simeq (\pi/2n\lambda')^{1/2} e^{i(n\lambda' + \pi/4)} [1 - (\pi y)^{1/2} e^y \operatorname{erfc}(y^{1/2})], \tag{76}$$

where

$$y = n\lambda' \xi'^6/2i \tag{77}$$

and erfc is the complimentary error function.[16]

If $|y|$, as well as λ, is large compared to unity, then (76) reduces to

$$I_n \simeq (\tfrac{1}{2}\pi)^{1/2} \frac{\exp[i(n\lambda' + \tfrac{1}{4}\pi)]}{(n\lambda')^{3/2} \xi'^6}, \quad \lambda, |y| \gg 1. \tag{78}$$

This harmonic oscillation with respect to $n\lambda = nL\omega_c/v$, with an amplitude varying as $L^{-3/2}$, is the result obtained by Gantmakher and Kaner[10] for the case where that section of the Fermi surface that had the extremal velocity in the direction of the magnetic field also had a finite cross section.

For the case where $|y|$ is not large, we let

$$y^{1/2} = (\pi/2i)^{1/2} x, \quad \text{or} \quad x = (n\lambda' \xi'^6/\pi)^{1/2} \tag{79}$$

and use the identity relating the erfc to the Fresnel integrals[16]

$$\operatorname{erfc}[(\pi/2i)^{1/2} x] = 1 - (2/i)^{1/2} [C(x) + iS(x)], \tag{80}$$

[15] G. A. Baraff, Phys. Rev. **178**, 1155 (1969).
[16] *Handbook of Mathematical Functions*, edited by M. Abramowitz and I. A. Stegun (U. S. Department of Commerce, National Bureau of Standards, Washington, D. C., 1964), Appl. Math. Ser. 55, Chap. 7.
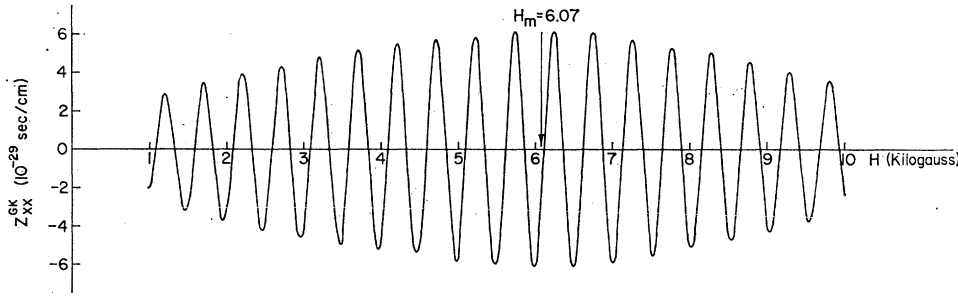
FIG. 8. Plot of the contribution of the first reflection of the GK contribution to the surface impedance Z_{xx} for parameters (50) in the collisionless limit $(\omega_c \tau \to \infty)$. The magnetic field at the edge $H = H_m$ is indicated. *Note added in proof.* The magnitude of the surface impedance is incorrect. It should be greater by a factor of 1.1×10^8 than that indicated in the figure.

to rewrite (76) as

$$I_n \simeq (\pi/2n\lambda')^{1/2} e^{i(n\lambda' + \pi/4)}$$
$$\times [1 - \pi x f(x) + i\pi x g(x)], \quad \lambda \gg 1 \quad (81a)$$

where the auxilliary functions[16]

$$f(x) = [\tfrac{1}{2} - S(x)] \cos(\tfrac{1}{2}\pi x^2)$$
$$- [\tfrac{1}{2} - C(x)] \sin(\tfrac{1}{2}\pi x^2), \quad (81b)$$

$$g(x) = [\tfrac{1}{2} - C(x)] \cos(\tfrac{1}{2}\pi x^2)$$
$$+ [\tfrac{1}{2} - S(x)] \sin(\tfrac{1}{2}\pi x^2), \quad (81c)$$

are monotonically decreasing for real x and are tabulated in Ref. 16.

Combining (81) with (67) we have for the nth reflection of the branch-cut contribution to the surface impedance in the $\lambda \gg 1$ limit

$$Z_+^{GK(n)} = (Z_-^{GK(n)})^*$$

$$= \frac{16i\omega \xi^3 v}{c^2 \omega_c (1 + i\eta)^4} \left(\frac{\pi}{2n\lambda'}\right)^{1/2} e^{i(n\lambda' + \pi/4)}$$

$$\times [1 - \pi x f(x) + i\pi x g(x)]. \quad (82)$$

The expression (82) is particularly useful in the collisionless limit $(\eta \to 0, x \text{ real})$, where it exhibits the real and imaginary parts of the surface impedance directly. These are plotted in Fig. 8 for the leading reflection $(n = 1)$ and the parameters (50), except that we now take the collisionless limit $(\eta = 1/\omega_c \tau \to 0)$. For the $\omega_c \tau$ value of (50) and the sample thickness, we have been using, $L = 0.1$ cm, we have $\lambda = 12.5H$ and $L/l = 0.63$, so the contributions of the successive reflections fall off as $\exp[-0.63n]$. That is, the nth term is about one-half of the $(n-1)$th term. For smaller more realistic τ values, the higher reflections will be damped out more rapidly.

We can look analytically at the high and low magnetic field behavior of the amplitude of the GK oscillations. Thus, for large magnetic field $(\omega_c \to \infty)$, Eqs. (75) and (76) are valid. For this limit we have $y \to 0$, so (76) implies

$$|I_n| \sim \omega_c^{-1/2}, \quad \omega_c \to \infty \quad (83)$$

and hence by (67) and (72) the part of the surface impedance due to the nth reflection of the GK contribu-

tion vanishes as

$$|Z_\pm^{GK(n)}| \sim \omega_c^{-5/2}, \quad \omega_c \to \infty. \quad (84)$$

For low magnetic fields one must be careful because lifetime effects become important as $\omega_c \to 0$. [We still assume $\omega \ll \omega_c$ as indicated after (38).] Let us first consider the case where ω_c is small so that $\xi^3 \gg 1$, but τ is sufficiently large so that $\eta \ll 1$. In this limit, we have from (73)

$$I_n \to \int_1^\infty dz \frac{(z^2 - 1)^{1/2}}{z^4(z^2 - 1) + \xi^6} e^{in\omega_c Lz/v} e^{-nLz/l}, \quad (85)$$

so that we have the inequality

$$|I_n| < \frac{1}{\xi^6} \int_1^\infty dz (z^2 - 1)^{1/2} e^{-nLz/l} = \frac{l}{\xi^6 nL} K_1(nL/l), \quad (86)$$

where K_1 is a modified Bessel function of the second kind. As the only ω_c dependence in (86) is in ξ^6, we have, with (67) and (72), the low-field result

$$|Z_\pm^{GK(n)}| < C\omega_c^2, \quad \omega_c \to 0, \quad \text{but} \quad \eta \ll 1, \quad (87)$$

where C is independent of magnetic field.

Thus, this contribution to the surface impedance gets small in both the high and low magnetic field limit. The amplitude of these oscillations must, consequently, have a maximum for intermediate fields (as shown in Fig. 8). Although the position of this maximum amplitude is difficult to obtain analytically, its frequency dependence is not. If we take the square of the real part of (82) and average it over the magnetic field oscillations, the resulting function will be proportional to the square of the amplitude. To find the maximum of the amplitude we must set the derivative of this function with respect to magnetic field equal to zero. However, in the collisionless limit, the magnetic field appears only in the combination given by x in Eq. (79), and the only additional frequency dependence occurs as a multiplicative factor. That is, the amplitude squared is equal to a function of ω times a function of x. The maximum with respect to magnetic field then occurs for x equal to some frequency-independent numerical value. Thus, if we vary the frequency, the magnetic field at the maximum amplitude

must vary in such a way as to keep x constant; that is, the magnetic field must vary as $H \sim \omega^{2/5}$. Experimentally, Weisbuch and Libchaber[17] found, for copper in the [111] direction, that the field at the maximum amplitude varied as $\omega^{1/3}$ (although $\omega^{2/5}$ also fits the data). We wish to emphasize, however, that this behavior is extremely model-dependent, and for a square root singularity will depend on other parts of the Fermi surface as well. Thus, if other parts of the Fermi surface give a contribution $g(z)$ to the conductivity in addition to the square root singularity, then instead of the appropriate parameter being $x \sim \lambda \xi^6$, it will involve $\lambda \xi^6 [1 - \xi^3 g(1)]^{-2}$ and one gets a rather different behavior. For singularities other than a square root (see Sec. VIII), the behavior will again be different. [The fact that the amplitude maximum in Fig. 8 occurs near the edge H_m is fortuitous. Since $H_m \sim \omega^{1/3} L^0$ while the magnetic field at the amplitude maximum varies as $\omega^{2/5} L^{1/5}$, these two fields would be separated for different values of the parameters.]

For sufficiently small fields, $|Z_\pm^{\mathrm{GK}(n)}|$ does not vanish as suggested by (87) because lifetime effects become important. [For the parameters (50), this should occur for $H \sim 0.1$ kG.] In this case, η is no longer negligible and, in fact,

$$\xi'^6 = \xi^6/(1+i\eta)^6 \to -(\xi/\eta)^6(1+6i/\eta), \quad \omega_c \to 0, \quad (88)$$

where ξ/η is independent of ω_c [and equal to about 90 for the parameters (50)]. In this limit the GK contribution to the surface impedance ceases to oscillate and approaches a constant independent of field. The contribution of the nth reflection to the total surface impedance behaves like

$$Z_+^{\mathrm{GK}(n)} + Z_-^{\mathrm{GK}(n)} \to (-1)^n \frac{16\pi}{3c} \left(\frac{\omega^2 v}{\omega_p^2 c} \right)^{1/3} e^{-n(L/l)(\xi/\eta)},$$

$$\omega_c \to 0. \quad (89)$$

For the parameters (50), the exponential in (89) makes this contribution quite small.

It will be noted that the GK contribution to the surface impedance in (89) is pure real. This is in fact a more general result to which we will now turn. Basically the point is that the two different polarizations set up GK oscillations with opposite phase velocities (see Fig. 3). In this linearly polarized excitation, the two polarizations combine so as to give only a real surface impedance due to the GK oscillations. To see how this comes about, we note that time reversal invariance, or explicit reference to (22), implies that

$$\sigma_\mp^*(-q, -\omega) = \sigma_\pm(q, \omega), \quad (90)$$

where we only take the complex conjugate of the functional form of the conductivity, not of its arguments.

The same result is true for the dielectric constant (7). From this it follows that

$$T_-^*(-\omega) = T_+(\omega). \quad (91)$$

Now, to be able to talk only about the GK contribution one must be able to separate the branch-cut contributions from the pole contributions. We have previously seen how to do this in our case, and since the branch cuts are entirely a property of the conductivity (90) [unlike the position of the poles (41)], we may write for the GK contribution alone

$$[T_-^{\mathrm{GK}}(-\omega)]^* = T_+^{\mathrm{GK}}(\omega). \quad (92)$$

Since, for the frequencies we have been considering, T_-^{GK} is odd in ω, we have

$$T_-^{\mathrm{GK}}(\omega) = -[T_+^{\mathrm{GK}}(\omega)]^* \quad (93)$$

and hence,

$$Z_-^{\mathrm{GK}} = (Z_+^{\mathrm{GK}})^*, \quad (94)$$

so that for linearly polarized excitation the surface impedance (48)

$$Z_{xx}^{\mathrm{GK}} = \tfrac{1}{2}(Z_+^{\mathrm{GK}} + Z_-^{\mathrm{GK}}) = \mathrm{Re} Z_+^{\mathrm{GK}} \quad (95)$$

is pure real.

Now, experimentally[10] one observes GK oscillations in $\mathrm{Im} Z_{xx}$. There are a number of reasons why this may happen. First, there are various experimental problems: The sample may not have parallel surfaces so that it is not excited symmetrically, or the alignment is not directly along a symmetry direction so that the circularly polarized modes do not quite diagonalize the conductivity. More important, however, is the fact that we have been assuming specular reflection. This assumption was critical in order to allow us to neatly separate the modes, and hence deduce (92) from (91). For the case of diffuse reflection[18] the strength of the branch-cut contributions depends on the pole terms and one cannot separate the modes so neatly. Since the pole terms are drastically affected when the sign of ω is reversed, we can no longer write (92). This difference between specular and diffuse reflection seems to be due to the fact that for specular reflection, electrons carrying a given mode are only excited at the surface by that same mode. The effect of fields due to other modes vanishes by interference between the approach to the surface and the reflection from the surface. For diffuse reflection, however, electrons leaving the surface have no recollection of their trip to the surface, and hence, they experience the entire field due to all modes without interference. The experimental observation of GK oscillations in $\mathrm{Im} Z_{xx}$ argues that the electrons do not undergo pure specular reflection at the surface, but (95) suggests that the GK oscillations should be more easily detected through the use of circularly polarized excitation.

[17] G. Weisbuch and A. Libchaber, Phys. Rev. Letters **19**, 498 (1967).

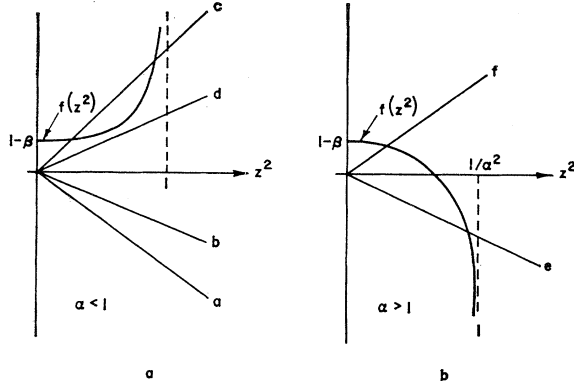[18] G. A. Baraff, Phys. Rev. **167**, 625 (1968).

FIG. 9. Graphical solution of (98) for $\beta<1$. Figure 9(a) corresponds to $\alpha<1$. Curves a and b are the left-hand side of (98) for $+$ polarization for high and low magnetic fields, respectively. Curves c and d are the left-hand side for $-$ polarization for high and low magnetic fields, respectively (above and below the edge). Figure 9(b) corresponds to $\alpha>1$, with curve e for $+$ polarization and curve f for $-$ polarization. For $\omega\ll\omega_c$, there is always one solution for each polarization.

VII. COMPENSATION EFFECTS: HIGH-FREQUENCY HELICONS IN METALS

The Fermi-surface model (23) was suggested by copper in the [111] direction. Copper, however, has hole orbits which partially compensate the electron orbits for fields in this direction. In order to see the kind of phenomena that may be produced by partial compensation, we consider, for simplicity, that the electron surface is that given by (23), while the hole surface is of the same form but with different parameters. Using subscripts e and h to denote, respectively, electron and hole parameters, the conductivity for this partially compensated model is then (for $\omega\ll\omega_{ce},\omega_{ch}$)

$$\sigma_{\pm}=\sigma_{\pm}^{e}+\sigma_{\pm}^{h}=\pm\frac{i}{4\pi}\left(\frac{\omega_{pe}^{2}}{\omega_{ce}[(1\pm i\eta_{e})^{2}-(qv_{e}/\omega_{ce})^{2}]^{1/2}}\right.$$
$$\left.-\frac{\omega_{ph}^{2}}{\omega_{ch}[(1\mp i\eta_{h})^{2}-(qv_{h}/\omega_{ch})^{2}]^{1/2}}\right). \quad (96)$$

Here ω_{ce} and ω_{ch} are both taken positive and we explicitly exhibit all signs which differ for electrons and holes. If we define the dimensionless quantities

$$z=qv_{e}/\omega_{ce}, \quad \xi^{3}=\omega\omega_{pe}^{2}v_{e}^{2}/\omega_{ce}^{3}c^{2}, \quad (97)$$

in terms of the electron parameters (arbitrarily), the dispersion equation (35) for the collective modes becomes (in the collisionless limit $\eta_{e},\ \eta_{h}\to0$)

$$\mp z^{2}/\xi^{3}=f(z^{2}), \quad (\pm\text{polarization}), \quad (98)$$

where

$$f(z^{2})=(1-z^{2})^{-1/2}-\beta(1-\alpha^{2}z^{2})^{-1/2}, \quad (99)$$

with

$$\alpha=\frac{v_{h}/\omega_{ch}}{v_{e}/\omega_{ce}}=\left(\frac{\partial A_{h}}{\partial p_{z}}\right)_{\text{ext}}\bigg/\left(\frac{\partial A_{e}}{\partial p_{z}}\right)_{\text{ext}} \quad (100)$$

and

$$\beta=n_{h}/n_{e}. \quad (101)$$

That is, α is the ratio of the extremal derivatives of the cross-section areas of the hole and electron surfaces, while β is the ratio of carrier densities.

If $\beta=1$, the system is exactly compensated and $f(0)=0$. This situation produces Alfvén waves rather than helicons.[7] We shall not treat this case here but confine ourselves to the situation where $|1-\beta|$ is not much smaller than unity. We assume the electrons are the majority carrier,

$$\beta<1. \quad (102)$$

This entails no loss of generality since the case $\beta>1$ would merely correspond to letting $\alpha\to1/\alpha$ and interchanging the two polarizations.

There are two qualitatively different cases, corresponding to $\alpha<1$ and $\alpha>1$. We again plot the left- and right-hand sides of the dispersion equation as functions of z^{2} (Fig. 9). For $\alpha<1$ [Fig. 9(a)], the behavior is similar to the uncompensated case: No real roots exist for the wrong ($+$) polarization (as always, we take $\omega>0$), while for the correct ($-$) polarization there is a critical field H_{m} which separates the high-field region ($H>H_{m}$, $\xi<\xi_{m}$), for which there are two real roots, from the low-field region ($H<H_{m}$, $\xi>\xi_{m}$), for which there are no real roots. The effect of compensation is simply to lower the edge field H_{m} somewhat. For very high fields the helicon obeys the classical uncompensated helicon dispersion equation (52) except that ω_{p}^{2} is replaced by $\omega_{pe}^{2}(1-\beta)$. That is the charge density n is replaced by $n_{e}-n_{h}$.
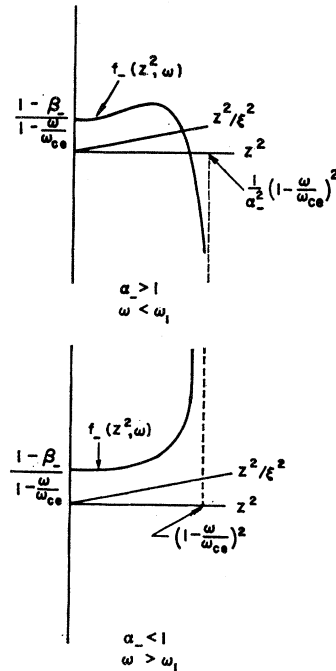

FIG. 10. Graphical solution of (103) for $-$ polarization showing the disappearance of the root. Figure 10(a) for $\alpha_{-}>1$, and $\omega<\omega_{1}$, shows one root. Figure 10(b) for $\alpha_{-}<1$ and $\omega>\omega_{1}$ shows none.

For $\alpha > 1$ [Fig. 9(b)], the situation is qualitatively different. Here there is one root for *each* polarization for *all* values of the magnetic field. [Provided that $\omega \ll \omega_{ce}$, ω_{ch} so that (96) is valid. See below for discussion of larger ω.] At high fields the $-$ polarization root is the ordinary (predominantly electron) helicon, while the $+$ polarization root lies close to the DSCR for *holes*. Figure 9(b) indicates that both these roots remain no matter how small the magnetic field. That is, since $f(z^2)$ can vanish for $\alpha > 1$, it follows from (98) that there is a root for either polarization corresponding to infinitely large ξ^3. From (97) we see that large ξ^3 corresponds to either small ω_{ce} (small magnetic field) or large ω. Thus, (98) implies that there are propagating modes in this partially compensated metal for vanishingly small magnetic fields or infinitely large frequencies (note that we only require $1 > \beta > 0$, so the carrier density $n_e(1-\beta)$ $= n_e - n_h$ can still be of metallic densities).

This result is valid only provided $\omega \ll \omega_{ce}$, ω_{ch}. When this condition is no longer valid, we must use a more accurate form of the conductivity than (96). Without assuming small frequencies, but still in the collisionless limit and ignoring Fermi-liquid effects, the dispersion equation (98) is replaced by

$$\mp z^2/\xi^3 = f_\pm(z^2,\omega), \quad (\pm\text{polarization}), \quad (103)$$

where

$$f_\pm(z^2,\omega) = [(1\pm\omega/\omega_{ce})^2 - z^2]^{-1/2} - \beta[(1\mp\omega/\omega_{ch})^2 - \alpha^2 z^2]^{-1/2}. \quad (104)$$

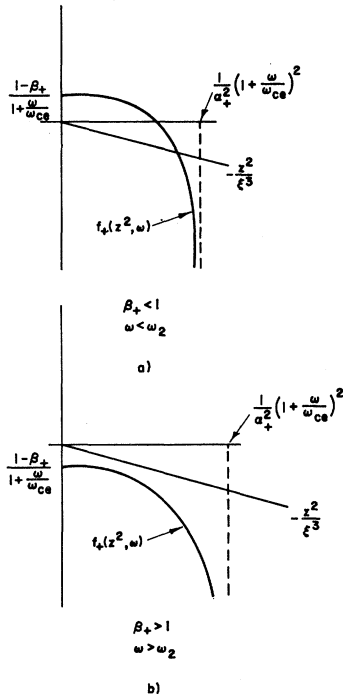FIG. 11. Graphical solution of (103) for $+$ polarization showing the disappearance of the root. Figure 11(a) for $\beta_+ < 1$ and $\omega < \omega_2$, shows one root. Figure 11(b), for $\beta_+ > 1$, $\omega > \omega_2$, shows none. The cutoff frequency is actually somewhat larger than ω_2.
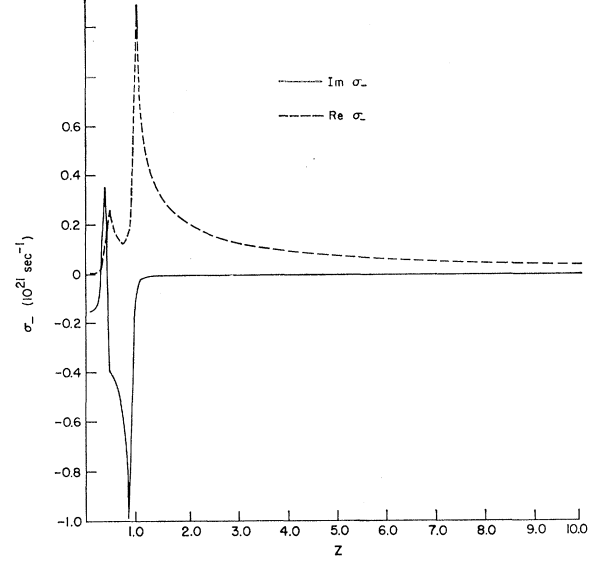
FIG. 12. Plot of the real and imaginary parts of the conductivity σ_- as a function of z, Eq. (97), for the parameters (111), and a magnetic field $H = 5$ kG.

It is convenient to rewrite (104) as

$$f_\pm(z^2,\omega) = [(1\pm\omega/\omega_{ce})^2 - z^2]^{-1/2} - \beta_\pm[(1\pm\omega/\omega_{ce})^2 - \alpha_\pm^2 z^2]^{-1/2}, \quad (105)$$

with

$$\alpha_-/\alpha = \beta_-/\beta = (1-\omega/\omega_{ce})/(1+\omega/\omega_{ch}),$$
$$\alpha_+/\alpha = \beta_+/\beta = (1+\omega/\omega_{ce})/(1-\omega/\omega_{ch}). \quad (106)$$

If $\alpha > 1$ and ω is increased (holding the magnetic field fixed), eventually $\alpha_-(\omega)$ will become equal to unity at some frequency $\omega = \omega_1$. Thus, for $-$ polarization, for $\omega < \omega_1$, there will be a real root for $z^2/\xi^3 = f_-(z^2,\omega)$ as seen in Fig. 10(a), while for $\omega > \omega_1$ the graphs of z^2/ξ^3 and $f_-(z^2,\omega)$ will not intersect, as seen in Fig. 10(b).[19]

The limiting frequency ω_1 is determined by

$$1 = \alpha_-(\omega_1) = \alpha(1 - \omega_1/\omega_{ce})/(1 + \omega_1/\omega_{ch}) \quad (107)$$

or

$$\omega_1 = \frac{\omega_{ce}\omega_{ch}}{\omega_{ce} + \alpha\omega_{ch}}(\alpha - 1) = \frac{\omega_{ce}v_h - \omega_{ch}v_e}{v_e + v_h}, \quad (108)$$

where use has been made of (100). Note that ω_1 depends linearly on H.

For the $+$ polarization, the root disappears when $\beta_+(\omega) \gtrsim 1$ so that $-z^2/\xi^3$ and $f_+(z^2,\omega)$ no longer intersect (Fig. 11). There is thus a cutoff frequency at a value somewhat larger than ω_2, where

$$1 = \beta_+(\omega_2) = \beta(1 + \omega_2/\omega_{ce})/(1 - \omega_2/\omega_{ch}), \quad (109)$$

[19] There is the possibility that there will still be two roots for $\omega > \omega_1$, but this requires very small ξ^3, corresponding to extremely high magnetic fields, $\omega_c \sim \omega_p v/c$ or $H \sim 10^4$ kG.
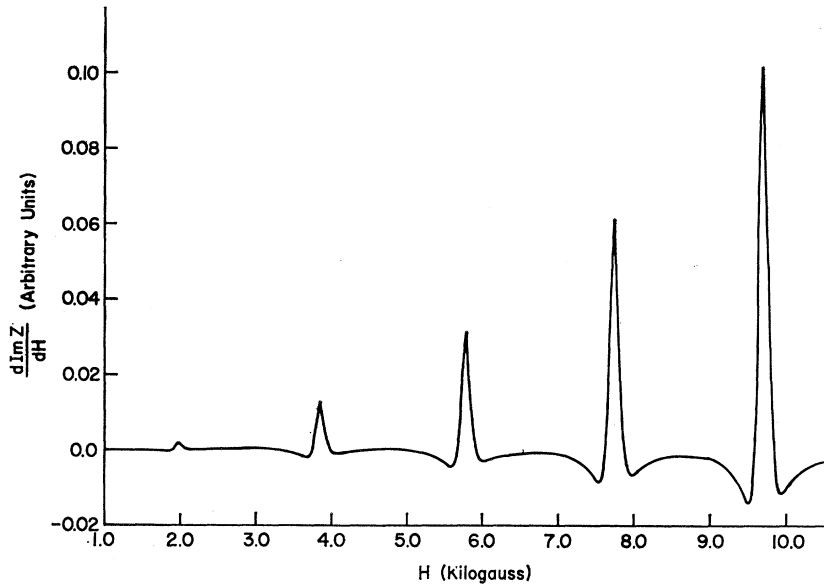
FIG. 13. Plot of the magnetic field derivative of the imaginary part of the surface impedance, as a function of magnetic field for − polarization, using the parameters (111).

or

$$\omega_2 = \frac{\omega_{ce}\omega_{ch}(1-\beta)}{\omega_{ce}+\beta\omega_{ch}} = \omega_{ce}\omega_{ch}\left(\frac{n_e-n_h}{n_e\omega_{ce}+n_h\omega_{ch}}\right), \quad (110)$$

where we have used (101).

As long as α and β are not too close to unity, ω_1 and ω_2 will have the order of magnitude of the cyclotron frequencies, and thus high-frequency helicons (microwave) are possible in partially compensated metals at reasonable magnetic fields. Helicons at these frequencies and fields can occur in semimetals[20] and semiconductors[21] because the density of carriers is low (in our model this is equivalent to $\omega_{pe}^2(1-\beta)$ being very small). The metallic high-frequency helicons discussed here are due to a rather different phenomenon, as seen in Fig. 9.

To exhibit this explicitly, we have evaluated the surface impedance (or rather its magnetic field derivative, the more commonly measured quantity) for this partially compensated model using the following parameters:

$$\omega = 2\pi\times10^9 \text{ sec}^{-1},$$

$$L = 0.1 \text{ cm},$$

$$v_e = 1.1\times10^8 \text{ cm/sec},$$

$$\omega_{pe}^2 = 2.7\times10^{32} \text{ sec}^{-2}, \quad\quad (111)$$

$$\omega_{ce} = \omega_{ch} = 1.38H\times10^{10} \text{ sec}^{-1},$$

$$\eta_e = \eta_h = 1/(20H),$$

$$\alpha = 3, \quad \beta = \tfrac{2}{3},$$

where, as usual, H is measured in kG. In Fig. 12, the conductivity σ_-, is plotted as a function of z, (97), for a field of 5 kG, showing the reversal of sign of $\text{Im}\sigma_-$ at

[20] M. S. Khaikin, V. S. Edelman, and R. T. Mina, Zh. Eksperim. i Teor. Fiz. 44, 2190 (1960) [English transl.: Soviet Phys.—JETP 17, 1470 (1963)].
[21] A. Libchaber and R. Veilex, Phys. Rev. 127, 774 (1962).

z a little less than 0.3, where $\text{Re}\sigma_-$ is still small. In Fig. 13 we show the magnetic field derivative of the imaginary part of the surface impedance for the case of the − polarization. The helicon peaks are clearly exhibited (quite sharp for this small value of η). The fact that the spacing between these peaks is relatively independent of field is due to the almost vertical $\text{Im}\sigma_-$, where it crosses the axis. That is, the value of z at the root of (103) does not change much with field. For the parameters chosen there is also a root to (103) for the + polarization, and in Fig. 14 we show the magnetic field derivative of the imaginary part of the surface impedance for the case of linear polarization, which by (48) is just one-half the sum of the contributions for the two circular polarizations. The double peaks correspond to one root of (103) for each polarization.

The low-field loss of the peaks is due to the cutoffs discussed above. When ω becomes equal to $\omega_1(H)$, the − polarization helicon is lost. For the parameters (111), this will occur, by (108) when $H = 0.91$ kG, so there should be no helicons below this field. Similarly ω will be equal to $\omega_2(H)$, according to (110), when $H = 2.31$ kG and the + polarization root should disappear at a somewhat lower field.

Finally, we should comment on lifetime effects. At these high frequencies the helicon root is close to $z = z_0$, the point where $f_-(z^2,\omega)$ vanishes (see Fig. 10). For infinite lifetime, $\text{Re}\sigma_-$ would be zero until $z = (1+\omega/\omega_{ch})/\alpha$, where the first square root singularity occurs in σ_-. In order that $\text{Re}\sigma_-$ should still be small at z_0 for finite lifetime, the spacing between these two points should be somewhat larger than η, i.e.,

$$(1+\omega/\omega_{ch})/\alpha - z_0 \gtrsim \eta. \quad\quad (112)$$

Now,

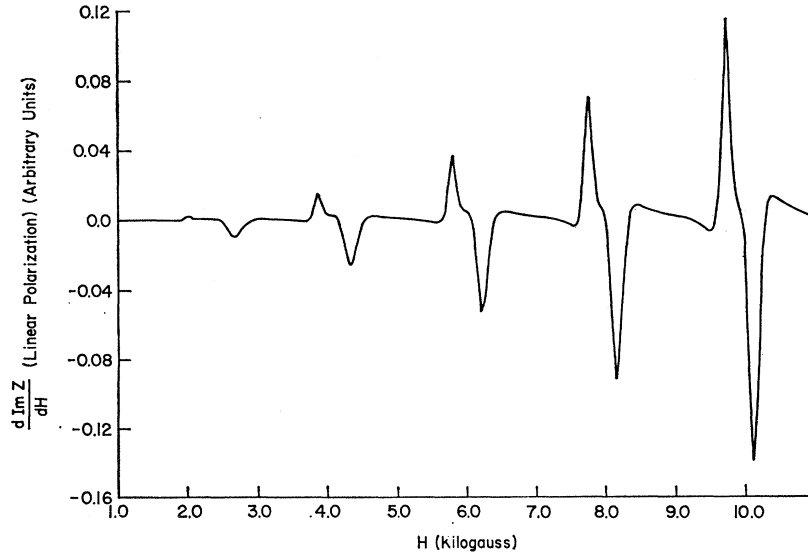$$z_0^2 = \frac{(1+\omega/\omega_{ch})^2 - (1-\omega/\omega_{ce})^2\beta^2}{(\alpha^2-\beta^2)}. \quad\quad (113)$$

FIG. 14. Same as Fig. 13, but for linear polarization.

Hence, to first order in η, (112) implies that $\mathrm{Re}\sigma_-$ will be small at the helicon root providing

$$\eta \lesssim \frac{\beta^2}{2\alpha(\alpha^2-\beta^2)} \frac{(1-\omega/\omega_{ce})^2\alpha^2-(1+\omega/\omega_{ch})^2}{1+\omega/\omega_{ch}}. \quad (114)$$

For the parameters (111), this implies that lifetime effects will be negligible for the helicon providing $H \gtrsim 2$ kG. Thus, for these parameters, lifetime effects become significant only where the helicon is already disappearing because $\omega \sim \omega_1(H)$.

VIII. OTHER MODELS: HIERARCHY OF SINGULARITIES

We turn now to a discussion of a variety of Fermi surfaces, most derived from the basic model (23), in order to exhibit some details that are model dependent. The basic model (23) had a square root singularity in its conductivity (32). That is, it had a square root branch point occurring when (for negligible ω and η)

$$qv = \pm\omega_c, \quad (115)$$

the condition for Doppler-shifted cyclotron resonance to occur. The nature of this branch point was intimately connected with the fact that the surface (23) has a velocity extremum, a point where $\partial v_z/\partial p_z = 0$, and that this point occurs where the cross-section area A is finite but where $|p_z|$ has not taken on its maximum value. This point is $p_z = \frac{1}{2}k$ (also $-\frac{1}{2}k$), where

$$A(\pm\frac{1}{2}k, \mu) = 2m\pi(\mu - vk/\pi) \quad (116)$$

and $|p_z|$ ranges continuously from 0 to k. (See Fig. 2.)

We shall see that the nature of the branch point (which affects the amplitude of the GK oscillations) depends on whether or not there is such an extremum, whether or not A vanishes at that point, and whether

or not that point is a $|p_z|$ endpoint. To demonstrate this with specific models, we can adjust the parameters in (23), as well as removing certain portions of the resultant Fermi surface. (This latter might correspond to the occurrence of Brillouin-zone boundaries, or to the interruption of one kind of orbit due to the presence of other sections of the Fermi surface. Thus, the six additional necks that copper has would interrupt some of the orbits of the kind we have been studying.)

We will therefore consider, briefly, eight different models. Five of these, labeled $A-E$, are derived from (23). Two, D' and E', are derived from a Fermi sphere and are only included because they are more familiar, not because they have any significant difference from models D and E. Finally, we include model F, previously considered by Skobov,[22] which exhibits no branch point and hence no GK oscillations.

Thus, models $A-E$ all have the same surface equation (23)

$$E = p_\perp^2/2m + (2/\pi)kv \sin^2(\pi p_z/2k). \quad (117)$$

Model A is the basic model with $\mu > 2vk/\pi$ [Fig. 15(a)]. Model B is a truncated version of model A with $0 \leq |p_z| \leq \frac{1}{2}k$ [Fig. 15(b)]. Model C is the same as B except that the cross-section area at $|p_z| = \frac{1}{2}k$ is adjusted to be zero, that is, $\mu = vk/\pi$ [Fig. 15(c)]. Model D is the same as model A except that the regions around the velocity extrema have been symmetrically removed. That is, the regions $\frac{1}{2}k(1-2\delta/\pi) \leq |p_z| \leq \frac{1}{2}k(1+2\delta/\pi)$ have been removed, where $\delta < \frac{1}{2}\pi$ [Fig. 15(d)]. Model E has $\mu < vk/\pi$ so that the cross-section area vanishes, and the Fermi surface terminates at a value $|p_z| = vk/\pi < \frac{1}{2}k$ [Fig. 15(e)]. (For $v = \frac{1}{2}\pi$ model E reduces to model C.)

Model E' is just the Fermi sphere with

$$E = p_\perp^2/2m + p_z^2/2m \quad (118)$$

_____

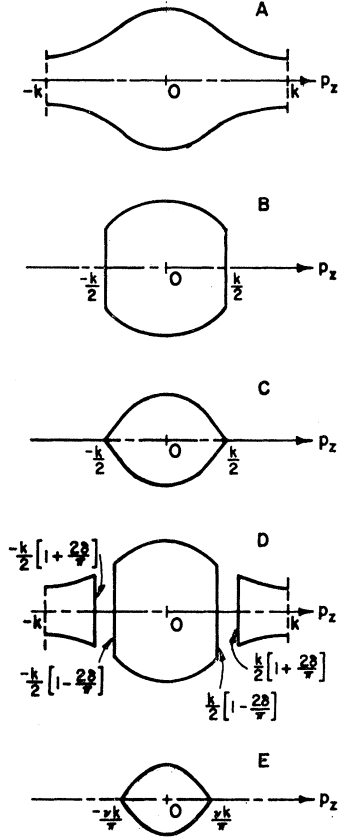[22] V. G. Skobov (private communication).

FIG. 15. Variety of Fermi surfaces based on (23). Part A is the basic model ($\mu > 2vk/\pi$) and is also depicted in Fig. 2. Part B is truncated at $|p_z| = \frac{1}{2}k$. Part C has $\mu = vk/\pi$. Part D has the regions $k(1-2\delta/\pi) \leq 2|p_z| \leq k(1+2\delta/\pi)$ removed. E has $\mu < vk/\pi$.

while Model D' is the same thing truncated so that $0 \leq |p_z| \leq p_0 < p_F$. Finally, Model F has

$$E = p_\perp^2/2m + v|p_z|. \tag{119}$$

The significant aspects of these models are as follows:

(a) Is there a point p_0 where $|v_z|$, or more precisely $|\partial A/\partial p_z|$ (these are the same thing for all these models because ω_c is independent of p_z) has a local maximum?

(b) Is the maximum $|\partial A/\partial p_z|$ an extremum? That is, does $(\partial^2 A/\partial p_z^2) = 0$? (This is as opposed to $|\partial A/\partial p_z|$ being maximal because it is increasing and p_z terminates at p_0.)

(c) Does $A(p_0) = 0$?

(d) Does $|p_z|$ terminate at p_0?

In Table I, we summarize this information together with the conductivity and the nature of the branch point for each of these models. We let

$$z_\pm = qv/\Omega_\pm, \tag{120}$$

with $\Omega_\pm$ given by (29) and for models D' and E' we let $v = p_F/m$. For model B, we introduce the parameter

$$a = [1 + \tfrac{1}{2}\pi(\pi\mu/vk - 1)]^{-1}, \tag{121}$$

which equals unity in the limit of model C. The ω_p^2 is that appropriate to each model.

There are thus three kinds of branch points exhibited. The strongest of these singularities is the square root (models A and B). This occurs when there is a concentration of electron orbits with almost the same $(\partial A/\partial p_z)|_E$ $[(\partial^2 A/\partial p_z^2)|_{p_0} = 0]$ at a point of finite cross section $[A(p_0) \neq 0]$, that is when there are enough electrons with orbits in the vicinity of p_0 to give a large contribution to the conductivity. If, however, there is no concentration of electron orbits with the same maximum $(\partial A/\partial p_z)|_E$ or the point of maximum $|(\partial A/\partial p_z)|_E|$ does not correspond to a finite cross section, then fewer electrons will contribute at this point and one only gets a logarithm (models D or C). If there is neither a concentration of orbits nor a finite cross section, there are only vanishingly few electrons to contribute and the singularity is still weaker, corresponding to a logarithm whose coefficient vanishes at the branch point. That is, there is no branch point in $\sigma_\pm$, only in $\partial\sigma_\pm/\partial z_\pm$. We have designated this kind of singularity a weak log (model E). It is weakest of all singularities, but it is the most familiar as it occurs for the Fermi sphere (model E').

We note that the singularity always occurs at the point of maximum $|(\partial A/\partial p_z)|_E| \sim |v_z|$. Thus, in model D there is no singularity at $z_\pm = \pm 1$, but rather at the branch point of the inverse tangent at

$$(1 - z_\pm^2)^{1/2} \cot\delta = \pm i, \tag{122}$$

which can be written in the form

$$qv \cos\delta = \omega_c(1 \pm i\eta). \tag{123}$$

Since $v \cos\delta$ is the maximum value of $|v_z|$ for this surface, (123) is seen to be the condition for Doppler-shifted cyclotron resonance for the electrons with maximum v_z. Similarly, the singularity for model E occurs when

$$qv \sin\nu = \omega_c(1 \pm i\eta) \tag{124}$$

and $v \sin\nu$ is the maximum $|v_z|$ for this surface, while for model D', the maximum $|v_z|$ is vp_0/p_F, and the singularity is displaced accordingly.

This indicates that by having an even greater number of electron orbits concentrated around the maximum v_z, we should be able to get an even stronger singularity. Model F has all electrons with the same $|v_z|$, and here the singularity is so strong that it is a pole, and there is no branch cut, and hence no GK oscillations. This behavior will occur if there is a finite region of constant $\partial A/\partial p_z$ on the Fermi surface.

The surface impedance for model F can easily be evaluated as there are only pole contributions. From (34) and (49) one gets

$$Z_\pm = -(2\pi i\omega v/c^2\omega_c)\{[1 + (1 \pm 4\xi_\pm^3)^{-1/2}](1/z_{\pm1})$$
$$\times \tan(\tfrac{1}{2}\lambda z_{\pm1}) + [1 - (1 \pm 4\xi_\pm^3)^{-1/2}]$$
$$\times (1/z_{\pm2})\tan(\tfrac{1}{2}\lambda z_{\pm2})\}, \tag{125}$$

Table I. Conductivities and branch points for various model Fermi surfaces.

Model	$\dfrac{\partial^2 A}{\partial p_z^2}\Big\|_{p0}$	$A(p_0)$	$\|p_z\|$ terminates at p_0?	Conductivity $\sigma_\pm$	Branch point
A	0	$\neq 0$	No	$\dfrac{i}{4\pi}\dfrac{\omega_p^2}{\Omega_\pm}(1-z_\pm^2)^{-1/2}$	Square root
B	0	$\neq 0$	Yes	$\dfrac{i}{4\pi}\dfrac{\omega_p^2}{\Omega_\pm}\left\{(1-a)[1-z_\pm^2]^{-1/2}+\dfrac{a}{2z_\pm}\ln\left(\dfrac{1+z_\pm}{1-z_\pm}\right)\right\}$	Square root and log
C	0	0	Yes	$\dfrac{i}{4\pi}\dfrac{\omega_p^2}{\Omega_\pm}\dfrac{1}{2z_\pm}\ln\left(\dfrac{1+z_\pm}{1-z_\pm}\right)$	log
D	$\neq 0$	$\neq 0$	Yes	$\dfrac{i}{4\pi}\dfrac{\omega_p^2}{\Omega_\pm}\dfrac{[1-z_\pm^2]^{-1/2}}{\frac{1}{2}\pi-\delta}\tan^{-1}[(1-z_\pm^2)^{1/2}\cot\delta]$	log
E	$\neq 0$	0	Yes	$\dfrac{i}{4\pi}\dfrac{\omega_p^2}{\Omega_\pm}\dfrac{1}{\sin\nu-\nu\cos\nu}\left\{\dfrac{1}{2z_\pm}\ln\left(\dfrac{1+z_\pm\sin\nu}{1-z_\pm\sin\nu}\right)\right.$ $\left.-\cos\nu(1-z_\pm^2)^{-1/2}\tan^{-1}[(1-z_\pm^2)^{1/2}\tan\nu]\right\}$	Weak log
D'	$\neq 0$	$\neq 0$	Yes	$\dfrac{i}{4\pi}\dfrac{\omega_p^2}{\Omega_\pm}\dfrac{1}{(1-p_0^2/3p_F^2)}\left\{\dfrac{1}{z_\pm^2}+\left(1-\dfrac{1}{z_\pm^2}\right)\dfrac{p_F}{2z_\pm p_0}\ln\left(\dfrac{1+z_\pm p_0/p_F}{1-z_\pm p_0/p_F}\right)\right\}$	log
E'	$\neq 0$	0	Yes	$\dfrac{i}{4\pi}\dfrac{\omega_p^2}{\Omega_\pm}\dfrac{3}{2}\left\{\dfrac{1}{z_\pm^2}+\left(1-\dfrac{1}{z_\pm^2}\right)\dfrac{1}{2z_\pm}\ln\left(\dfrac{1+z_\pm}{1-z_\pm}\right)\right\}$	Weak log
F	All p_z have same $\|v_z\|\left(\sim\left\|\dfrac{\partial A}{\partial p_z}\right\|\right)$			$\dfrac{i}{4\pi}\dfrac{\omega_p^2}{\Omega_\pm}\dfrac{1}{1-z_\pm^2}$	None

where

$$\xi_\pm^3 = (\omega_p^2\omega v^2/\omega_c^3 c^2)(1\pm i\eta)^{-3}, \qquad (126)$$

and the $z_{\pm j}$ are the positions of the upper-half plane poles for the $\pm$ polarization. They are given by

$$z_{\pm 1} = (1\pm i\eta)[\tfrac{1}{2}-\tfrac{1}{2}(1\pm 4\xi_\pm^3)^{1/2}]^{1/2}, \qquad (127)$$

$$z_{\pm 2} = \pm(1\pm i\eta)[\tfrac{1}{2}+\tfrac{1}{2}(1\pm 4\xi_\pm^3)^{1/2}]^{1/2}, \qquad (128)$$

where the phases of the square roots must lie between $-\pi$ and π. For the $-$ polarization the situation is familiar. The helicon root is z_{-1} and the DSCR root is z_{-2}. In the collisionless limit the helicon edge occurs as $\xi = \xi_m$ where

$$\xi_m^3 = \tfrac{1}{4}. \qquad (129)$$

For the $+$ polarization, z_1 is the usual damped helicon root, but z_2 is a new kind of root occurring because model F has a pole singularity instead of a branch point. This means that, in the collisionless limit, for $z^2 > 1$, Reσ_+ remains zero, but Imσ_+ becomes negative. There is thus always a solution, denoted z_2, to the dispersion relation (35) for the $+$ polarization, corresponding to $z^2 > 1$. We can understand this negative Imσ_+ as follows. Since half the electrons have the same velocity v in the z direction (the others have $v_z = -v$), we can use a frame of reference moving with them. In this frame, the electromagnetic field appears to have a frequency approximately equal to qv. When $qv > \omega_c$, the electrons cannot

keep up with the applied field, and thus find themselves responding 180° out of phase. That is, they behave as if they had the opposite charge, and hence the conductivity goes negative. For the usual Fermi surface, the same situation would ensue for each value of v_z on the Fermi surface, and we would have a dense set of poles, one for every v_z at $qv_z = \omega_c$. Thus, for a continuous range of v_z we get a branch cut. In model F, however, all the electrons move together. Now, in the frame of these electrons, large qv corresponds to large ω, and hence as qv gets very large, the conductivity must vanish, as the electrons can not follow the applied field at all. This means that the larger the q value of the applied field, the smaller the interaction of it with the electrons. Now, as the magnetic field is increased, the propagating mode z_2 moves to lower q, approaching the resonance at $q = \omega_c/v$. This mode will then interact more and more with the electrons as the field is increased, and we expect the surface impedance to decrease. This is seen from (125), which implies that the z_2 contribution to Z_+ diminishes for large H as ω_c^{-4}. In Fig. 16, we have plotted the magnetic field derivative of ImZ_+ for model F for the parameters (50) but with $\omega_c\tau = 5H$, and this phenomenon is clearly exhibited. The slight fall-off just apparent at low fields is due to lifetime effects becoming important as $(\omega_c\tau)^{-1}$ becomes large. Finally, in Appendix B, we examine the edge anomaly in Z_- for model F for both specular and diffuse boundary conditions.
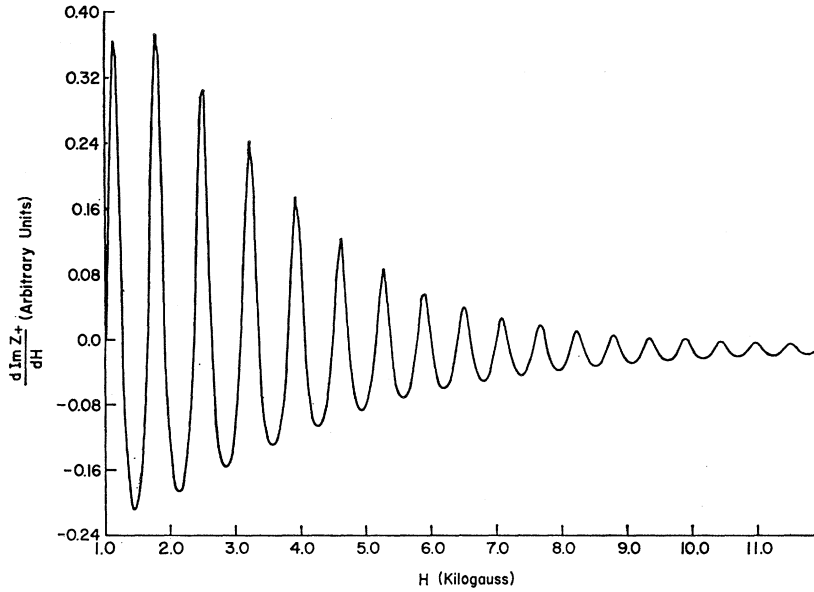
FIG. 16. Plot of the magnetic field derivative of the imaginary part of the surface impedance for model F, as a function of magnetic field for $+$ polarization, using the parameters (50) but with $\omega_c \tau = 5H$.

The above discussion of branch points has been in terms of specific models, but the results are model-independent. We can see this by writing the conductivity (22), at zero frequency, for a general Fermi surface having cylindrical symmetry about the direction of the magnetic field (the z direction)[12,6]

$$\sigma_{\pm}(q) = \pm \frac{2}{(2\pi)^3} \frac{iec}{H}$$

$$\times \int_{\text{FS}} dp_z \frac{A(p_z)}{1 \pm i\eta \mp (qc/2\pi eH)(\partial A/\partial p_z)|_E}. \quad (130)$$

The integral is over the Fermi surface. We note that, by (22a) and (22b),

$$\frac{c}{2\pi eH} \frac{\partial A}{\partial p_z}\Big|_E = -\frac{c}{2\pi eH} \frac{\partial A}{\partial E}\Big|_{p_z} \frac{\partial E}{\partial p_z}\Big|_A = -\frac{v_z}{\omega_c}. \quad (131)$$

Thus, insofar as ω_c is constant over the Fermi surface, as it is for all our models, we may discuss v_z and $(\partial A/\partial p_z)|_E$ interchangeably, as we have been doing. If ω_c is not constant, then (130) indicates that the important parameter is $(\partial A/\partial p_z)|_E$. Hence, for example, conical surfaces of constant energy would give a constant $|v_z|$, but not a constant ω_c, so they would not result in a simple pole singularity as model F does with its constant $|v_z|$ and ω_c.

We now expand $A(p_z)$ and $(\partial A/\partial p_z)|_E$ about p_0, a point of maximum $|(\partial A/\partial p_z)|_E|$. Then,

$$A(p_z) = A^{(0)} + (p_z - p_0)A^{(1)} + \frac{1}{2}(p_z - p_0)^2 A^{(2)}$$

$$+ \frac{1}{6}(p_z - p_0)^3 A^{(3)} + \cdots, \quad (132)$$

$$\frac{\partial A}{\partial p_z}\Big|_E = A^{(1)} + (p_z - p_0)A^{(2)} + \frac{1}{2}(p_z - p_0)^2 A^{(3)} + \cdots, \quad (133)$$

where

$$A^{(n)} = \frac{\partial^n A}{\partial p_z^{n}}\Big|_{E, p_z = p_0}. \quad (134)$$

The predominant contribution to $\sigma_{\pm}$ will be from p_z near p_0 [and near any other values at which $|(\partial A/\partial p_z)|_E|$ is a maximum] and that contribution is then (letting $k \equiv p_z - p_0$)

$$\Delta\sigma_{\pm}(q) = \pm \frac{2}{(2\pi)^3} \frac{iec}{H} \int_{\Delta k} dk$$

$$\times \frac{A^{(0)} + kA^{(1)} + \cdots}{1 \pm i\eta \mp (qc/2\pi eH)(A^{(1)} + kA^{(2)} + \frac{1}{2}k^2 A^{(3)} + \cdots)}, \quad (135)$$

where Δk is a region around $k = 0$. If $|p_z|$ terminates at p_0, then one of the limits of integration in (135) will be $k = 0$, otherwise Δk can be taken as a symmetric region around $k = 0$. We note that by (131)

$$\mp (qc/2\pi eH)A^{(1)} = \pm (qv_z/\omega_c)|_{p_0}. \quad (136)$$

Hence, for there to be a singularity at

$$(qv_z/\omega_c)|_{p_0} = \pm 1 + i\eta, \quad (137)$$

we must have $A^{(1)} \neq 0$. If one keeps the first nonvanishing term in the numerator and the denominator of (135), it is straightforward to get the leading singularity at the point (137). Using the second, third, and fourth columns of Table I in (135) one easily gets the branch points given in the last column. (Of course, for model B, only the leading square root is obtained. To get the logarithm, one must also keep the $A^{(1)}$ term in the numerator.) One can then go on to complete the hierarchy of singularities.

If

$$A^{(0)}\neq 0, \quad A^{(1)}\neq 0, \quad A^{(2)}=A^{(3)}=\cdots=A^{(n)}=0,$$

$$A^{(n+1)}\neq 0, \quad n\geq 2 \tag{138a}$$

then the leading singularity is given by

$$\sigma_{\pm}\sim [1\pm i\eta\pm(qv_z/\omega_c)_{p_0}]^{-(n-1)/n} \tag{138b}$$

and if

$$A^{(0)}=0, \quad A^{(1)}\neq 0,$$

$$A^{(2)}=A^{(3)}=\cdots=A^{(n)}=0, \quad A^{(n+1)}\neq 0, \quad n\geq 2 \tag{139a}$$

then the leading singularity is given by

$$\sigma_{\pm}\sim [1\pm i\eta\pm(qv_z/\omega_c)_{p_0}]^{-(n-2)/n}. \tag{139b}$$

In (139b), if $n=2$, the power of zero in the singularity is understood to imply a logarithm.

These differences in branch-point singularities are reflected in the dependence of the amplitude of the GK oscillations on the sample thickness. Thus, the first reflection of the GK contribution to the surface impedance is proportional to [generalizing (73)] the integral

$$I_1 = \int_{\Gamma} dz \frac{e^{i\lambda' z}}{z^2 - \xi^3 f(z)}, \tag{140}$$

where $f(z)$ has the singularity of the conductivity (138b), (139b), or the appropriate logarithmic singularity for cases like models C through E' (Table I). The contour Γ goes in a counterclockwise direction around the branch cut, which has been rotated to lie along the real axis between $z=1$ and $z=\infty$. We let

$$f(z)=f_1(z), \quad \text{above the cut}$$
$$f(z)=f_2(z), \quad \text{below the cut.} \tag{141}$$

Then,

$$I_1 = \int_1^{\infty} dz e^{i\lambda' z} \frac{\xi^3(f_2-f_1)}{z^4 - z^2\xi^3(f_1+f_2)+\xi^6 f_1 f_2}. \tag{142}$$

For thicker samples (λ sufficiently large), the dominant contribution to (142) comes from z near unity. If $f(z)$ diverges at $z=1$, as it does for all singularities except the weak logarithm, the last term in the denominator dominates.

If we consider the case of (138), then

$$f(z)\sim(1-z)^{-1+(1/n)}, \quad n\geq 2 \tag{143a}$$

and for large λ, (142) gives

$$I_1\sim e^{i\lambda'}/(\lambda')^{2-1/n}, \quad n\geq 2. \tag{143b}$$

A special case of this is $n=2$, where we have the familiar square root. Equation (143b) then gives an amplitude proportional to $\lambda'^{-3/2}$ in agreement with (78). For the case of (139), we have

$$f(z)\sim(1-z)^{-1+(2/n)}, \quad n>2 \tag{144a}$$

and for large λ, (142) gives

$$I_1\sim e^{i\lambda'}/(\lambda')^{2-2/n}, \quad n>2. \tag{144b}$$

The logarithmic and weak logarithmic singularities must be treated separately. The use of (142) for the logarithm requires some care (it involves Ramanujan's integral[23]), but ultimately one gets

$$I_1\sim e^{i\lambda'}/\lambda' \ln^2\lambda', \quad \text{logarithm.} \tag{145}$$

For the weak logarithm, it is the first term in the denominator of (142) that dominates, and one gets

$$I_1\sim e^{i\lambda'}/\lambda'^2, \quad \text{weak logarithm.} \tag{146}$$

This last result, as well as (143b) for $n=2$, was obtained by Gantmakher and Kaner in their original paper.[10]

As a final comment, we note that, in the entire hierarchy of singularities given in Table I and (138) and (139), only in the case of the weak logarithm does $\sigma_{\pm}$ remain finite when the condition for Doppler-shifted cyclotron resonance is satisfied. In all other cases, $\sigma_{\pm}$ diverges.[24] This means that when we consider the dispersion relation for the collective modes of the electromagnetic field (35), we shall find that the frequency ω will vanish (see Fig. 6) at $(qv_z/\omega_c)_{p_0}=1$, in all cases except that of the weak logarithm. Only for the weak logarithm does the dispersion relation not bend over all the way to zero. Thus, the Fermi sphere (which, because there are vanishingly few electrons at the limiting point to contribute, has a weak logarithmic singularity) can be viewed as the most anomalous case.

ACKNOWLEDGMENTS

APPENDIX A

We wish here to evaluate the integrals I_n, Eq. (73), in the limit $\lambda\gg1$. To do this, we distort the line of integration from the real axis to the line A as indicated in Fig. 17. In doing this we will pickup the contribution of any poles that lie between the original contour and line A, as well as the integral along line A, which we denote by J_n. Thus,

$$I_n = J_n + (\text{pole contributions}) \tag{A1}$$

Along line A, we can write

$$z = 1 + is/n\lambda', \tag{A2}$$

[23] *Bateman Manuscript Project*, edited by A. Erdélyi (McGraw-Hill Book Co., New York, 1953), Vol. III.
[24] *Note added in proof.* Of course, for finite τ the conductivity $\sigma_{\pm}$ remains finite for all models.
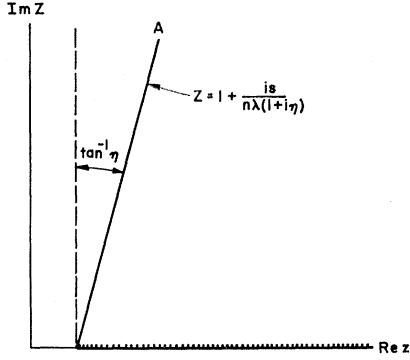
FIG. 17. Plot of the contours of integration used in evaluating I_n (73). The dotted line is the original contour of integration; line A is the distorted contour. Any poles lying between these contours will contribute.

where s is a real parameter. Then,

$$J_n = \frac{ie^{in\lambda'}}{n\lambda'} \int_0^\infty ds \frac{[(2is/n\lambda') - (s^2/n^2\lambda'^2)]^{1/2}e^{-s}}{[1+is/n\lambda']^6 - [1+is/n\lambda']^4 + \xi'^6}. \quad (A3)$$

Retaining only the leading terms in inverse powers of λ', we have

$$J_n \simeq \frac{ie^{in\lambda'}}{(2in\lambda')^{1/2}} \int_0^\infty ds \frac{s^{1/2}e^{-s}}{s+y}, \quad (A4)$$

where

$$y = n\lambda'\xi'^6/2i. \quad (A5)$$

The integral in (A4) is easily evaluated in terms of the complementary error function[16] to give

$$J_n \simeq \left(\frac{\pi}{2n\lambda'}\right)^{1/2} e^{i(n\lambda'+\pi/4)}[1-(\pi y)^{1/2}e^y \operatorname{erfc}(y^{1/2})]. \quad (A6)$$

Now, there will be a pole contribution if the magnetic field is such that one of the roots of the denominator of (73),

$$z^6 - z^4 + \xi'^6 = 0 \quad (A7)$$

lies to the right of line A in the upper-half plane. However, in order for this to occur, that root must be so far from the real axis that the residue will be strongly damped. Its contribution may therefore be neglected and we may take

$$I_n \simeq J_n, \quad (A8)$$

giving the result (76).

APPENDIX B

We wish here to compare the edge anomaly for model F (119), for the cases of specular and diffuse boundary conditions. As in Sec. V, we evaluate the surface impedance in the limit of an infinitely thick sample so that the edge anomaly is not obscured by the geometrical resonances. We look at the $-$ polarization, as that is the polarization for which the edge exists. Evaluating the specular reflection result (125) in the $\lambda \to \infty$ limit gives

$$Z_-^{\mathrm{SR}} = \frac{2\sqrt{2}\pi\omega v}{c^2\omega_c(1-i\eta)}$$
$$\times \left(\frac{[1+(1-4\xi_-^3)^{1/2}]^{3/2} + [1-(1-4\xi_-^3)^{1/2}]^{3/2}}{2\xi_-^{3/2}(1-4\xi_-^3)^{1/2}}\right). \quad (B1)$$

In the vicinity of the edge, we have

$$|1-4\xi_-^3| \ll 1, \quad (B2)$$

so

$$Z_-^{\mathrm{SR}} \simeq \frac{4\sqrt{2}\pi\omega v}{c^2\omega_c(1-i\eta)}(1-4\xi_-^3)^{-1/2}. \quad (B3)$$

This has the same kind of behavior as model A had [see Eq. (64) and Fig. 5].

For diffuse-reflection boundary conditions, the surface impedance for an infinitely thick sample is given by[1]

$$Z_-^{\mathrm{DR}} = -\frac{4\pi i\omega}{c^2}\left\{\int_0^\infty dq \ln\left[1-\frac{4\pi i\omega}{q^2c^2}\sigma_-(q)\right]\right\}^{-1}. \quad (B4)$$

For model F, this is easily evaluated to give

$$Z_-^{\mathrm{DR}} = \frac{4\omega v}{\omega_c c^2(1-i\eta)}\{1+(1/\sqrt{2})[1-(1-4\xi_-^3)^{1/2}]^{1/2}$$
$$-(1/\sqrt{2})[1+(1-4\xi_-^3)^{1/2}]^{1/2}\}^{-1}, \quad (B5)$$

which, near the edge (B2), reduces to

$$Z_-^{\mathrm{DR}} \simeq [4\omega v/\omega_c c^2(1-i\eta)][1+(1/\sqrt{2})(1-4\xi_-^3)^{1/2}]. \quad (B6)$$

This has rather different behavior than the specular case (B3), the square root appearing there in the denominator and here linearly.

The anomalies in these two cases appear the same as Alig[14] found for a Fermi sphere (weak logarithm), and thus would seem to depend more on the boundary conditions than on the shape of the Fermi surface.